Published in final edited form as:
J Chem Theory Comput. 2007 ; 3(6): 1927–1946. doi:10.1021/ct700100a.

Polarizable empirical force field for the primary and secondary alcohol series based on the classical Drude model

Victor M. Anisimov[1], **Igor V. Vorobyov**[1], **Benoît Roux**[2], and **Alexander D. MacKerell Jr.**[1*,†]

1*Department of Pharmaceutical Sciences, School of Pharmacy, University of Maryland, 20 Penn Street, Baltimore, MD, 21201*

2*Institute of Molecular Pediatric Sciences, Gordon Center for Integrative Science, University of Chicago 929 E. 57th St. Chicago, IL 60637*

Abstract

A polarizable empirical force field based on the classical Drude oscillator has been developed for the aliphatic alcohol series. The model is optimized with emphasis on condensed-phase properties and is validated against a variety of experimental data. Transferability of the developed parameters is emphasized by the use of a single electrostatic model for the hydroxyl group throughout the alcohol series. Aliphatic moiety parameters were transferred from the polarizable alkane parameter set, with only the Lennard-Jones parameters on the carbon in methanol optimized. The developed model yields good agreement with pure solvent properties with the exception of the heats of vaporization of 1-propanol and 1-butanol, which are underestimated by approximately 6%; special LJ parameters for the oxygen in these two molecules that correct for this limitation are presented. Accurate treatment of the free energies of aqueous solvation required the use of atom-type specific $O_{alcohol}$-O_{water} LJ interaction terms, with specific terms used for the primary and secondary alcohols. With respect to gas phase properties the polarizable model overestimates experimental dipole moments and quantum mechanical interaction energies with water by approximately 10 and 8 %, respectively, a significant improvement over 44 and 46 % overestimations of the corresponding properties in the CHARMM22 fixed-charge additive model. Comparison of structural properties of the polarizable and additive models for the pure solvents and in aqueous solution shows significant differences indicating atomic details of intermolecular interactions to be sensitive to the applied force field. The polarizable model predicts pure solvent and aqueous phase dipole moment distributions for ethanol centered at 2.4 and 2.7 D, respectively, a significant increase over the gas phase value of 1.8 D, whereas in a solvent of lower polarity, benzene, a value of 1.9 is obtained. The ability of the polarizable model to yield changes in dipole moment as well as the reproduction of a range of condensed phase properties indicates its utility in the study of the properties of alcohols in a variety of condensed phase environments as well as representing an important step in the development of a comprehensive force field for biological molecules.

Introduction

Alcohol moieties are one of the most ubiquitous classes of functional groups, representing building blocks of proteins, nucleic acids, lipids and carbohydrates as well as being found in a wide range of industrial chemicals, including pharmaceuticals. For example, hydroxyls are present in the amino acids serine, threonine and tyrosine, the presence of the hydroxyl group at the 2' position of the ribose ring in RNA leads to its unique properties as compared to DNA

*Corresponding author phone: (410) 706-7442; fax: (410) 706-5017; e-mail: alex@outerbanks.umaryland.edu.
†University of Maryland

and hydroxyls dominate the structure and function of carbohydrates. Notable is the presence of both polar and non-polar moieties in their structures, allowing alcohols to participate both in hydrophobic and hydrophilic interactions. To better understand the properties of alcohols a number of theoretical chemistry studies have been undertaken,[1–9] including empirical force field based studies investigating their condensed phase properties. To date a majority of these have been based on non-polarizable (fixed-charge additive) models, such as those available in the popular all-atom bio-molecular force fields CHARMM[10, 11], Amber[12], and OPLS-AA[4, 13], among others.[3, 14, 15] The additive models use fixed partial atomic charges and in all cases it is necessary to overestimate the gas phase dipole moment of alcohols by approximately 40 % in order to accurately treat the condensed phase (including alcohols in aqueous solution). Despite their usefulness, the assumption of additivity in the treatment of electrostatic interactions prevents an accurate treatment of the full range response in polar and nonpolar environments where the alcohol function groups exist in biomolecules. To overcome the limitation of additive empirical force fields, models that include explicit treatment of electronic polarizability are being developed and a number of classical polarizable models for alcohols have been presented.[16–23] These models have been based on induced dipoles[16–18, 24], fluctuating charges[20–22] and the Drude model[19, 23] to treat the electronic polarizability. In some of the models the internal parameters were transferred directly from the corresponding additive models with few remaining parameters being optimized to reproduce condensed-phase properties[18, 19, 24]. In other models parameters for hydroxyl groups are set to be unique for the particular alcohol being studied and can not be regarded as transferable across the alcohol series.[21–23] In the present work we extend these efforts via the development of a polarizable model for the alcohol series (Figure 1) with emphasis on maximizing the transferability of the developed parameters to biological macromolecules. In addition, a systematic, iterative approach is applied to rigorously optimize all aspects of the force field parameters to maximize the overall accuracy of the model.

The present work follows the hierarchical approach towards the optimization of force field parameters that was originally developed for the CHARMM all-atom biomolecular force field.[11] This work builds on the classical Drude polarizable models developed for water[25, 26], the alkane series,[27] aromatics[28] and ethers.[29] As before the optimization of all necessary parameters including atomic charges, atomic polarizabilities, internal equilibrium parameters, force constants, torsion potentials and Lennard-Jones terms is undertaken. In the polarizable alcohol series the alkyl group parameters are transferred directly from the alkanes with only the methyl group in methanol being partially optimized as described below.

Methods

The induced polarization framework employed in this work is based on the classical Drude oscillator model as described previously.[30] According to this model each non-hydrogen atom is described by two point charges q_{core} and δ connected by a harmonic spring with a force constant of k_D. The sum of the two point charges yields the partial atomic charge q_A associated with atom A (i.e., $q_A = q_{core} + \delta$). The host atom in the Drude model is also the center of the Lennard-Jones (LJ) radius whereas the Drude particle typically does not carry LJ parameters (although LJ parameter can be assigned in principle). Placement of atom in an external field E causes a displacement of the charged Drude particle, which gives rise to an induced dipole $\mu=\alpha E$; the displacement (x) of Drude particles from their corresponding atomic centers in response to the external field is opposed by the restoring force of the harmonic spring $F_{harm}= -k_D x$, which defines the polarizability $\alpha=\delta^2/k_D$ of an atom. When there are many polarizable atoms responding to a field E, the calculation of the total electrostatic interactions can be achieved by relaxing the charged Drude particles iteratively until self-consistency. Alternatively, in the case of MD simulations an extended Lagrangian may be applied allowing the treatment of the electronic degrees of freedom as dynamic variables.[30, 31]

Electrostatic interactions of Drude particles with other charged centers involving 1,4 pairs and beyond are treated according to Coulomb's Law as commonly used in classical force fields.[32] 1,2 and 1,3 intramolecular electrostatic interactions between covalently connected atoms, which are typically turned off in additive models, are reintroduced in the polarizable model at the level of dipole-dipole interactions. Here, the Drude particles inherit the position index of their corresponding host atoms. The presence of 1,2 and 1,3 dipole interactions increases the internal polarizability of molecules as well as the anisotropy of that polarizability.[33] Effective inclusion of the 1,2 and 1,3 interactions requires their scaling to avoid polarization catastrophe. Scaling is performed using the approach of Thole[34, 35] where the interaction energy of the induced dipoles on the atomic centers *i* and *j* is calculated according to the modified Thole scheme:

$$\frac{\delta_i \delta_j}{r_{ij}} \left[1 - \left(1 - \frac{\bar{r}_{ij}}{2} \right) \cdot \exp\left(-\bar{r}_{ij} \right) \right] \tag{1}$$

where the normalized distance is defined as

$$\bar{r}_{ij} = a \frac{r_{ij}}{\sqrt[6]{\alpha_i \alpha_j}} \tag{2}$$

and r_{ij} is the distance between the interacting centers, α_i is the atomic polarizability of center *i*, and *a* is a Thole parameter with a default value of 2.6, originally selected to produce the correct polarizability anisotropy ratio of benzene.[34, 35]

Optimization of the electrostatic parameters is performed using the FITCHARGE module in the program CHARMM[10, 11] and is an extension of our previously published protocol.[36] Modifications include the placement of an additional "near" grid and the inclusion of virtual charged particles at the position of oxygen lone-pairs (LP).[33] The effective charge of the oxygen atom is moved entirely to the corresponding LP sites (two LPs per oxygen atom), while the polarizability is retained on the atomic center. Initial optimization of charges and polarizabilities was done by fitting to quantum mechanical (QM) electrostatic potential (ESP) maps. One "unperturbed" EPS map is calculated for the isolated molecule of interest and a number of additional "perturbed" maps are calculated in the presence of small point charges (0.5*e*) placed at different locations to probe the polarization response. Grids defining the ESP were placed on concentric surfaces at multiples of the van der Waals (vdW) radii of atoms. The perturbating point charges as required for the production of perturbed ESPs are placed along bonds, and at additional locations to approximate an isotropic distribution around the molecule, using the parameters listed in Table 1. In Table 1 the vdW scale factor indicates the distance of the Connolly surfaces from the atomic centers in multiples of the corresponding atomic vdW radius. The total number of points on each surface is a multiple of the "density factor". The "distance to atoms" parameter does not allow placement of a perturbation ion or a grid point at a distance less than the specified value to any atom in the molecule. The "distance to perturbation ions" parameter prevents newly added perturbation ions being closer to other ions than the specified distance. Finally, "type" descriptor specifies the way the points are generated. The type "ions (bonds)" means that the perturbation ions are placed along vectors extended from covalent bonds while "ions (gaps)" places ions in vacant regions on a surface between the ions originally placed based on the bonds criteria. The type "grids" indicates placement of grid points. The present work extends our previous methodology by adding a layer (#1) of perturbation ions and a corresponding layer of grid points (#4) at a vdW scale factor of 1.3, thereby taking into account the electrostatic response at distances corresponding to direct hydrogen bonds, as described below. Further, an additional layer (#5) of grid points at distances corresponding to the separation of heavy atoms involved in hydrogen bonds was added.

Initial guesses of the charges for ESP fitting were based on the CHARMM22 force field.[11] Initial values for the polarizabilities were obtained from the additive atomic polarizabilities of Miller[37] modified for the present non-hydrogen polarizability model, as described previously.[36] Fitting was performed on monomer geometries optimized at the MP2(fc)/6-31G(d) level of theory[38] using the Gaussian 03 package[39] with ESPs calculated using the B3LYP functional[40–44] with aug-cc-pVDZ basis set.[45] Gauche- and trans-conformations of ethanol and iso-propanol were included in the fitting. The positions of the LPs were determined by varying the LP geometry to minimize the RMS error between the QM and empirical ESPs and to reproduce the relative interaction energies of alcohols with water for different orientations.

QM calculations of alcohol-water complexes were done by constraining the geometry of the alcohols to the corresponding MP2(fc)/6-31G(d) optimized geometry and water geometry to that of SWM4-NDP model[25]. The position of the water relative to the alcohol molecule was optimized at the MP2(fc)/6-31G(d) level of theory for the interaction distance, C-O…H_{water} angle, and H(O)…C-O…H_{water} torsion. Single point LMP2/cc-pVQZ[46, 47] calculations were performed on the minimum energy geometry to obtain the interaction energy using the program Jaguar (Schrodinger Inc.) as previously described.[48] Water-alcohol orientations used in the present study are shown in Figure 2. Empirical alcohol-water interactions were performed on preliminarily relaxed geometry of alcohols with the water orientation obtained from corresponding QM calculations. Only the interaction distance was optimized in the empirical calculations with other geometrical parameters held fixed at their initial values.

QM calculations of the alcohol complexes with rare gas atoms were performed using MP2(fc)/6-31G(d) optimized geometry of the corresponding alcohols. Relative position of rare-gas atom was adopted from alcohol-water interactions with additional positions added to probe the alkyl carbon atoms. Minimum interaction energies and distances for rare gas – alcohol complexes were determined using interaction distance scans with 0.01Å increments. Energy of the complex was evaluated at the MP3(fc)/6-311++G(3d,3p) level of theory for each point on the scan path.[49] The rare gas atom placement is illustrated in Figure 3.

Empirical force field calculations were performed with program CHARMM. Energy minimizations of model compounds in the gas phase were performed with the adopted basis Newton-Raphson minimizer (ABNR)[10, 50] to a final RMS gradient of 10^{-5} kcal/(mol * Å). All gas phase calculations were performed using infinite cutoffs.

Equilibrium parameters and force constants associated with the bonds, valence and torsion angles were optimized targeting the mean values of geometric parameters from the survey of crystal structures[51], QM geometries and QM vibrational spectra of the model compounds. The QM calculations were performed at the MP2/6-31G(d) level and a scale factor of 0.9434 was applied to vibrational modes to account for limitations in the level of theory.[52] Second derivatives of energy with respect to atomic coordinates of real atoms were obtained numerically with position of Drude particle self-consistently adjusted to every change in coordinates of the real atoms. Potential energy decomposition analysis was performed using the MOLVIB utility[53] in CHARMM. Internal coordinate assignment was done according to Pulay et al.[54]

Target data for optimization of the dihedral parameters were torsion energy profiles obtained from QM calculations. Dihedral angle scans were performed in 10° increments for the torsion angle with subsequent geometry relaxation performed at the MP2(fc)/6-31G(d) level, which was followed by single-point energy evaluation at the MP2/cc-pVTZ[55] level. A similar procedure was repeated in the force field calculations where the torsion angle of interest was scanned while other geometrical parameters were fully relaxed. Dihedrals were restrained to their target values using harmonic force constants of 10^5 kcal/(mol * $Å^2$) and energy

minimizations were performed with ABNR method to RMS gradients of 10^{-5} kcal/(mol * Å). Empirical torsion parameters were optimized to minimize the difference between the potential energy profile and the MP2/cc-pVTZ data.

Molecular dynamics (MD) simulations of condensed phases were performed at a constant pressure of 1 atm with cubic periodic boundary conditions using the velocity Verlet integrator that includes treatment of Drude particles via an extended Langrangian.[30] The integration time step was 1 fs for both polarizable and additive simulations with temperatures maintained at 298.15 K using the Nose-Hoover thermostat[56] with a relaxation time of 0.1 ps applied to all real atoms. A modified Andersen-Hoover barostat[30, 57] with a relaxation time of 0.1 ps was used to maintain the system at constant pressure. The SHAKE algorithm was used to constrain covalent bonds involving hydrogens.[58] Lennard-Jones (LJ) interactions were treated explicitly out to 12 Å with force switch smoothing[59] applied over the range of 10 to 12 Å. Nonbond pair lists were maintained out to 14 Å and the long range correction for LJ interactions[60] was applied in the condensed-phase simulations. Electrostatic interactions were treated using particle mesh Ewald (PME) summation[61] with a coupling parameter 0.34 and 6th order spline for mesh interpolation. The extended Lagrangian double-thermostat formalism[30] was used in all polarizable MD simulations where a mass of 0.4 amu was transferred from real atoms to the corresponding Drude particles. The amplitude of Drude oscillations was controlled with a separate low-temperature thermostat at 1 K to simulate near-SCF conditions.[30]

Pure solvent MD simulations included 128 alcohol molecules. To obtain convergent results 5 independent MD simulations were run for 250 ps with different initial velocities being assigned to the particles. The first 50 ps of the simulations were treated as equilibration and the final 200 ps were used for the analysis. Averages were obtained from the 5 independent simulation averages which were also used to calculate the standard errors for the calculated properties. Heats of vaporization, ΔH_{vap} and molecular volume V_m were determined following the standard procedure.[27] Gas-phase simulations were performed using Langevin dynamics in the SCF regimen with infinite cutoffs for nonbonded interactions. The friction coefficient of 5 ps^{-1} was applied to all atoms except for Drude particles. The gas-phase simulations were performed on all 128 individual monomers extracted from the respective equilibrated alcohol box from the condensed-phase MD simulations. The simulations were run for 250 ps for each molecule with the resultant energies obtained from last 200 ps. The gas-phase energy was the average of the averages from the 128 monomer simulations.

Radial distribution functions, isothermal compressibilities, and self-diffusivities were calculated for the alcohols from condensed-phase MD trajectories. Isothermal compressibilities were calculated from

$$\beta_T = -\frac{1}{V}\left(\frac{\partial V}{\partial P}\right)_T = \frac{\langle \partial V^2 \rangle}{\mathrm{V k}_B T} \tag{3}$$

according to Klauda et al.,[62] where V is the volume, $\langle \delta V^2 \rangle$ is the volume fluctuation, and k_B is Boltzmann's constant. The slope of the mean squared displacement versus time was used to determine the self-diffusivity for the periodic boundary condition, D_{PBC}. The self-diffusivity was corrected for system-size effects using the hydrodynamic model of Yeh and Hummer[63] of a particle surrounded by a solvent with viscosity, η,

$$D_S = D_{\mathrm{PBC}} + \frac{k_B T \xi}{6\pi\eta L} \tag{4}$$

where L is the cubic box length and ξ=2.837297. The shear viscosities were taken at their experimental values.

Free energies of aqueous solvation (relative to gas phase), ΔG_{sol}, were obtained as a sum of nonpolar, ΔG_{np}, and electrostatic, ΔG_{elec}, contributions via a free energy perturbation (FEP) approach[64, 65] according to the step-by-step staged protocol developed by Deng and Roux.[66]

$$\Delta G_{sol} = \Delta G_{np} + \Delta G_{elec} \tag{5}$$

The nonpolar contribution was obtained from the perturbation formula[64, 65], where the free energy change ΔG, corresponding to the change in the potential energy from U_i to U_j, can be calculated as an average over the ensemble of configurations generated with the potential energy U_i:

$$\Delta G = -kT \ln\langle \exp\left(-\frac{U_j - U_i}{kT}\right)\rangle_{(U_i)} \tag{6}$$

The nonpolar contribution was calculated with all atomic and Drude charges of the solute set to 0. In the protocol the nonpolar term was decomposed into dispersive, U^{dis}, and repulsive contributions, U^{rep}, using the Weeks, Chandler, and Andersen scheme.[67]

$$U_{uv}^{np}(X,Y,\xi) = U_{uv}^{rep} + \xi U_{uv}^{dis}(X,Y) \tag{7}$$

The dispersive contribution was calculated using a linear coupling scheme with the coupling parameter ξ such that the interaction energy $U_{uv}(X,Y)$ between solute u with coordinates X and solvent v with coordinates Y was calculated as ξ was changed from 0 to 1 in increments of 0.1. The repulsive term, due to its sharp r^{12} dependence, cannot be treated accurately via a linear perturbation and instead was transformed into a soft-core potential. It was calculated in multiple stages with a staging parameter s. The staging parameter s was set to 0.0, 0.2, 0.3, 0.4, 0.5, 0.6, 0.7, 0.8, 0.9, and 1.0. The free energy contributions from simulations using different staging parameters were summed. The weighted histogram analysis method (WHAM)[68] was used to obtain the dispersive and repulsive contributions to free energies from the simulations. The electrostatic component of the free energy of hydration was computed by decoupling a molecule of the solute from the solvent by thermodynamic integration (TI)[69–71]:

$$\Delta G_{elec} = \int_0^1 d\lambda \langle \frac{dU(\lambda)}{d\lambda} \rangle \tag{8}$$

where the coupled state (λ=1) corresponds to a simulation where the solute is fully interacting with the solvent and the uncoupled state (λ=0) corresponds to a simulation where the solute dose not interact with the solvent. In the perturbations λ was changed from 0 to 1 in 0.05 increments with a 0.1 window size and half of the window overlapping with the previous window. Each contributing term to the free energy was obtained as a difference in the free energy of the solute in water and in vacuum.

For the free energy calculations gas-phase simulations were performed using Langevin dynamics with SCF Drudes as described above. Aqueous phase calculations were performed with the alcohol molecule solvated in a box of 250 SWM4-NDP polarizable water[26] molecules and restrained to the center of mass of the box by a harmonic potential with a force constant of 0.5 kcal/(mol * Å^2) acting on all solute atoms except Drudes. The system was then subjected to a 110 ps NPT simulation at 298.15 K and 1 atm pressure at each value of the coupling/staging parameter. The FEP analysis was performed on the final 100 ps of these dynamics runs. The reported free energy value was averaged over five independent runs each performed with individual seed numbers. Corresponding non-polarizable simulations were performed using the TIP3 water model.[72] During free energy calculation the molecular dynamics simulations did not include long-range correction (LRC) for dispersion forces. However, the latter were estimated from 50 ps MD simulations of a single alcohol molecule placed in a box of 250 water

molecules. The MD calculations were performed using the protocol described for simulations of the condensed phase. The energy due to LRC was calculated for the fixed configuration of the solute-solvent system as difference of the van der Waals energy contribution calculated using 10 and 30Å non-bonded cutoffs and averaged for 30 snapshots each written at 1 ps time intervals.

The static dielectric constants ε of the neat alcohols were calculated from the total

$$\varepsilon=\varepsilon_{\infty}+\frac{4\pi}{3\langle V\rangle k_B T}\left(\langle \mathrm{M}^2\rangle-\langle \mathrm{M}\rangle^2\right) \tag{10}$$

dipole moment M fluctuations of the box;[25, 30, 73] $\langle V\rangle$ is the average volume of the box, and ε_{∞} is the high-frequency dielectric constant. Time series of M were obtained from 5 independent simulations of 5 ns using data from the last 4 ns of each simulation following the previously discussed protocol.[27] The high-frequency contribution ε_{∞}, representing the dielectric constant at the limit of infinitely high frequency of light, is estimated from the Clausius-Mossotti equation:

$$\frac{\varepsilon_{\infty}-1}{\varepsilon_{\infty}+1}=\frac{4\pi\alpha}{3V_m} \tag{11}$$

where α is gas-phase molecular polarizability; V_m is molecular volume.

Results and Discussion

Optimization of the alcohol parameters targeted the compounds methanol, ethanol, and 2-propanol (isopropanol), with greater emphasis placed on ethanol for the primary alcohols. The derived parameters were then validated on 1-propanol, 1-butanol, and 2-butanol to test their transferability. This was followed by additional optimization on the oxygen LJ parameters for 1-propanol and 1-butanol to obtain better agreement with experimental molecular volume and enthalpy of vaporization (see below). The molecules, which include both primary and secondary alcohols, are shown in Figure 1. Hydroxyl groups located on tertiary carbon atoms are not common in biological macromolecules and, therefore, were not considered in this study. For the alcohol series the aliphatic carbon and hydrogen parameters previously determined in our laboratory[27] were applied directly with the exception of the electrostatic parameters on $CH_{(1–3)}$ fragments directly adjacent to the oxygen and of the LJ parameters for the methyl group in methanol. The remaining parameters were optimized as part of the present work.

The parameter optimization was performed using the following protocol. The electrostatic part of the polarizable model was initially derived from fitting to QM unperturbed and perturbed ESP maps with the geometry of the model compounds being fixed at their corresponding QM values. The internal parameters were initially taken from the additive CHARMM22 force field. Next, optimization of the LJ parameters was undertaken based on condensed-phase simulations and rare gas - model compound interactions. After the LJ parameters were initially determined (within 5% of target heat of vaporization and molecular volume) the internal parameters were updated to reproduce target geometries and vibrational spectra. Next the torsion parameters were optimized to reproduce the QM dihedral potential energy surfaces. After the first round of optimization was completed the atomic charges and polarizabilities were manually adjusted to reproduce QM data on interactions with water as well as dipole moments and condensed phase properties. The LJ parameters were then reoptimized and the internal parameters, including the dihedral parameters, were correspondingly updated. These steps were repeated until convergence.

Intramolecular parameters

Target data for the equilibrium bonded parameters were intramolecular geometries obtained from surveys of the Cambridge Crystallographic Database.[51] Structural data involving hydrogen atoms were obtained from MP2(fc)/6-31G(d) gas-phase optimized geometries. Equilibrium geometries of the model compounds for the final parameters are summarized in Table 2 along with the corresponding target data. The empirical model shows good overall agreement with the target data. The maximum deviation is 0.04 Å for C-C bond (C-COH) and 0.7 degrees for C-C-C angle. The C-C bond was not optimized due to adopting the hierarchical approach for parameter development requiring the parameters for the previously defined alkane atom types be preserved. Such constraint is an important precondition for maintaining transferability of the developed parameters and it also helps reduce the number of parameters to be optimized.

Reproduction of vibrational spectra along with potential energy surfaces for rotation about selected dihedrals was used to optimize the force constants. Presented in Table S1, S2 and S3 of the supporting information are the Drude and target QM vibrational spectra for methanol, ethanol and 2-propanol. Inspection of those results shows the agreement of both the magnitudes of the frequencies and the assignments to be excellent. The largest difference, the CO torsion in the IR-spectrum of methanol, was due to final adjustment of the associated parameter based on the energy surface, as follows. Final optimization of the dihedral parameters was based on the reproduction of QM energy surfaces. Shown in Figure 4 are the surfaces for the three molecules. It is evident that the Drude model satisfactorily reproduces the QM surfaces and is significantly better than CHARMM22, which was originally optimized targeting lower level QM data. The level of agreement of the Drude model for both the vibrational and dihedral surfaces indicates that the alcohols will sample the correct intramolecular conformations during MD simulations.

Electrostatic model

Atoms in classical molecular mechanics are traditionally treated as point charges. This leads to a certain degree of arbitrariness in the derivation of partial atomic charges from electrostatic fitting that cannot be eliminated due to the inherent ambiguities in partitioning the electron distribution with respect to a set of atomic centers. Therefore the point charge fitting to a QM electrostatic potential is often conducted under restraints enforcing that the derived charges follow chemical intuition.[74] The CHARMM additive force field[11] was developed according to a slightly different methodology. Because of the aforementioned limitations in the fitting of atomic charges to electron distributions, plus additional uncertainty as to how well gas-phase fitted charges would work in the condensed-phase, the additive CHARMM force field treated the atomic charges as adjustable parameters. These terms were then optimized to reproduce energetics and geometries of test molecules interacting with water along with condensed phase properties. This approach was successfully validated in the development of CHARMM22 and CHARMM27 additive force fields.[11, 75] In the classical Drude polarizable model the number of electrostatic parameters has increased due to the inclusion of atomic polarizabilities. To address this additional complexity the Drude electrostatic parameter determination protocol in CHARMM has been extended to include ESP fitting.[36] However, as the final goal of the resultant force field is the reproduction of condensed phase properties as well as atomic details of gas phase interactions with water, manual corrections of the ESP fitted values are considered acceptable.

An additional factor that has to be taken into account during the optimization of electrostatic parameters is the placement of virtual charged particles representative of oxygen lone pairs (LP). Inclusion of LPs was motivated by the inability of force field models without them to accurately reproduce the angular dependence of ESP maps in the case of hydrogen bond

acceptors.[33, 76] The charge on LP sites and their geometry were initially determined from the ESP fitting procedure to reduce the RMS error during fitting. The resulting fitted charges, polarizabilities and LP geometry were then tested on interactions with water and LP positions were further adjusted to better reproduce the local anisotropy of interactions with water. Because calculation of the interactions with water requires LJ parameters on the hydroxyl the CHARMM22 values were used as an initial guess. In later stages of the optimization the LP position and atomic charges were reevaluated based on interactions with water each time a new set of oxygen LJ parameters became available from the condensed-phase optimization (see below). This elaborate optimization procedure was performed for ethanol only with the derived LP positions applied without change to the other alcohols. The final oxygen lone pair position were as follows: distance between oxygen atom center and lone pair center = 0.35 Å; C-O-LP angle = 110°; virtual torsion angle H(O)-C-O-LP = ±91°.

Placement of water molecules around the hydroxyl group in the primary and secondary alcohols is illustrated on Figure 2 and the interaction energies and distances are presented in Table 3 and Table 4, respectively, for both the additive and polarizable models. Additive CHARMM22 force field results are presented as a representative example of those for an additive alcohol force field. Examination of the CHARMM22 energy differences, ΔE, show them to be significantly more favorable than the QM target data and the balance amongst the interaction orientations to be poor with the differences ranging from −0.6 to −2.2 kcal/mol for ethanol (Table 3). The more favorable interaction energies are expected given the need to overpolarize the effective fixed charges in the additive model to account for the lack of explicit polarizability. However, the limitation in the balance of the interactions for different placements of water molecule around the test molecule is due to limitations in the anisotropy of the electrostatic representation. This problem was also seen in the Drude model without LPs.[33] Therefore the Drude model of alcohols was extended to include LPs on the oxygen atom, yielding a more anisotropic electrostatic model. This anisotropy was further extended by assigning anisotropic polarizability on the oxygen atom. This anisotropic polarizability was introduced by treating the Drude force constant (k_D) of the oxygen as a tensor, as previously described.[33] The X-axis of the tensor is defined along C-O bond; the Y-axis goes through the oxygen atom perpendicular to the plane created by C-O-H atoms; the Z-axis is orthogonal to the X and Y axes. Increased stiffness of the Drude constant along the C-O bond (X-axis) reduces the overestimation of alcohol-water interaction in the 180-orientation (e.g. 180 in Table 3 for the C22 models). In addition, reducing the force constant along the Y-axis effectively increases oxygen polarizability along the lone-pair directions (e.g. 120 in Table 3 and Figure 2). More details of the impact of the inclusion of LPs and anisotropy on methanol and other molecules with hydrogen bond acceptors is presented in Harder et al.[33] Thus, by increasing the force constant along the X direction and decreasing it along the Y-axis leads to improvements in the balance of interactions of the hydroxyl with water. The final values of the tensor are k_{Dxx}=600, k_{Dyy}=400, k_{Dzz}=500 kcal/(mol * Å^2) with the same anisotropic Drude constants used for all the alcohols. In addition, the use of anisotropic polarizability leads to a more accurate representation of the polarization response around the hydroxyl group.[33]

As discussed above the additive model systematically overestimates the water-alcohol interactions energies (i.e. too favorable) and there is an imbalance in the treatment of the energies as a function of orientation. These effects are indicated by the large negative ΔE_{C22} values in Table 3 for the former and the greater values of the $RRMS_{C22}$ values for the latter in comparison with the polarizable model. In the Drude model both of these problems are largely alleviated. There is still a tendency for the interaction energies to be slightly too favorable, though the magnitude is generally much less than with the additive model. While such a problem may have contributions from the level of theory used in the *ab initio* calculations, the need to overestimate the interaction energies was necessary to obtain the correct pure solvent properties (see below). It should be noted that the data in Table 3 and Table 4 represent the use

off diagonal LJ terms for the $O_{hydroxyl}$—O_{water} interactions, as discussed in the following section. Ideally, the need to overestimate the gas phase interactions with water is not required for a polarizable model; future investigations will address this result. With respect to the balance of the interactions, the Drude model behavior is satisfactory, with the tendency to overestimate the 180-orientation significantly decreased with respect to the additive model. Thus, the polarizable alcohol model that incorporates oxygen atom charge anisotropy (due to LPs) and oxygen polarization anisotropy more accurately reproduces the change in interaction energy with water as a function of orientation as compared to the additive model.

Due to parameter correlation, the optimization of the electrostatic terms has to be repeated whenever the LJ parameters are changed, because new LJ parameters alter the interactions with water. Therefore, the LJ optimization from condensed phase simulations and electrostatic model optimization steps are repeated until convergence as judged by the agreement with the target condensed phase data typically being 2% or less. This iterative optimization procedure leads to maximizing agreement with the condensed phase properties while gas phase interactions are sacrificed to some extent. However, inclusion of the water interaction data assures that the model satisfactorily describes atomic details of hydrogen bonding as discussed above, an attribute that is anticipated to have paramount influence on the utility of the model in biomolecular simulations.

As mentioned above, small corrections to the ESP fitted charges were necessary during the parameter optimization. The manual adjustment of charges addresses two issues. First, it circumvents the present limitation that the ESP fitting procedure be applied to only one test molecule at a time (although simultaneous fitting of multiple conformations is performed in this work). Ideally, for a series of compounds for which transferable parameters are desired, they all should be fit simultaneously, including the application of equality restraints on those groups of atoms that should be transferable (e.g. the hydroxyl O and H atoms for the primary alcohols). The second issue is related to the requirement that the derived transferable charges and polarizabilities should ultimately reproduce as correctly as possible the interaction energies of the model compounds with water. Conceivably, one could implement an extended global optimization procedure simultaneously including the ESP for a set of molecules in multiple conformations as well as their interactions with water molecules in specific hydrogen binding configurations to achieve such goal. However, it is not trivial to perform such global optimization with all the different target data weighted appropriately. For the sake of simplicity, in the present work manual adjustment of the electrostatic parameters was performed, addressing the two issues in two steps. To evaluate the robustness of this approach as well as the transferability of the parameters additional calculations were performed on alcohols not included in the training set.

Another modification to the ESP fitting procedure[36] is the addition of several new Connolly surface layers for placement of perturbation ions and grid points. This was motivated by the inability of the published procedure to yield an electrostatic model that reproduced condensed-phase properties of alcohols. Application of the original approach produced electrostatic models that significantly (about 2 kcal/mol) underestimated the enthalpy of vaporization of ethanol (experimental value 10.11 kcal/mol), such that LJ parameter optimization could not correct the deficiency of the derived charge model. Comparison of the hydroxyl charges for the additive CHARMM22 (q_O=−0.66; q_H=0.43) with those derived using the original[36] grid (q_O=−0.436; q_H=0.312) indicates substantial underestimation of polarity of the hydroxyl group, leading to underestimation of the electrostatic contribution to the enthalpy of vaporization. To correct for this deficiency the fitting protocol was extended to include an additional “near” grid and perturbation ions in the vicinity of polar atoms thereby increasing the contribution of polar atoms in ESP fitting. The location of this grid is shown in Figure 5. The ethanol charges derived from the extended grid fitting procedure (q_O=−0.462; q_H=0.355)

show an increased local dipole of the hydroxyl group and indeed allowed identification of LJ parameters that yielded satisfactory condensed-phase properties. Despite the improvement brought by the near grid the fitting procedure gave different charges for methanol, ethanol, and 2-propanol (Table 5), whereas to enforce the parameter transferability a single set of charges was required. Therefore, the fitted charges and polarizabilities were subjected to manual adjustment, leading to the final optimized charges for alcohols of q_O=−0.46 (q_{LP}=−0.23); q_H=0.36, which are quite close to the ESP fitted values. Basically, the ESP fitting provided a good initial guess for the electrostatic model although empirical adjustment was required to derive the final fully balanced electrostatic model.

The final electrostatic parameters are presented in Table 6. Two additional adjustments were made to the electrostatic model prior to finalization. As discussed previously,[25, 26] it appears to be necessary to empirically scale gas phase polarizabilities by a factor smaller than 1.0 to yield accurate properties of polar molecules for the condensed phase. This was necessary for the SWM4-NDP water model and is applied to account for increased Pauli exclusion that occurs in the condensed phase due to surrounding molecules in the environment over that in the gas phase. Further support for the reduced polarizabilities are studies on macromolecules in the condensed phase, where unscaled values can lead to polarization catastrophe.[25, 77–79] Accordingly, the polarizabilities of aliphatic moieties in the alcohols were scaled by 0.7 consistent with the scaling applied to the SWM4-NDP water model. This yielded a polarizability of 1.4 for the CH_3 group (alkane value 2.05) and 1.2 for CH_2 group (alkane value 1.66). A sp3 carbon atom is considered an alkane type if it is not covalently bound to a heteroatom. The electronic properties of carbon atoms directly connected to heteroatoms are influenced by the electronegative character of such atoms and, therefore, are included in ESP fitting. Therefore, the polarizability of the carbon atom connected to oxygen was taken as the average from the ESP fitted values for methanol, ethanol, and 2-propanol and scaled by 0.7 giving the final polarizability value of 1.0. The oxygen atom was treated differently. Here the polarizability was set to the Miller value of 1.0[36] and not scaled as the unscaled value was required to reproduce the dipole moments, the interactions with water, and the condensed phase properties all in the context of enforcing transferability across the alcohols studied. Importantly, tests indicated that the oxygen polarizability was not causing electrostatic collapses in either the pure solvent or aqueous environment MD simulations.

Dipole moments for the final electrostatic models are shown in Table 7 along with CHARMM22 and target experimental and QM values. The fixed-charge additive CHARMM22 values are approximately 44% larger than the target values, which is necessary for the additive model to reproduce condensed phase properties. The agreement with experimental gas-phase dipole moments is improved in the polarizable model; however, the values are still overestimated by 10%. This is consistent with the polarizable model yielding more favorable interactions energies with water (Table 3) as required to reproduce the condensed phase properties throughout the alcohol series. A similar approach was utilized by Gao[18] in development of the PIPF polarizable model for alcohols by treating the dipole moment as an adjustable parameter to improve agreement with condensed-phase properties and is necessary to obtain the targeted condensed phase properties as discussed below.

Final atomic charges and polarizabilities, presented in Table 6, represent a balance required to reproduce target data of all alcohols throughout the series with primary importance in reproducing condensed-phase properties. Grid scans (Tables S8, S9 and S10, Supporting Information) of point charges and atomic polarizability parameters performed in the vicinity of the optimized parameter values confirm their optimal choice. Attempts to improve the agreement with the target data through variations of the charges do show improvement for individual properties but the overall agreement with the multiple target properties considered becomes poorer. For example, decreasing the value of point charges followed by a

corresponding increase in atomic polarizabilities would improve agreement with gas-phase dipole moment, but it would also negatively impact the already too favorable dielectric susceptibility of 1-butanol. Therefore, the current electrostatic parameters represent a balance for the entire alcohol series within the limitations of a transferable parameter set for the hydroxyl group. Such a constraint is a necessary prerequisite for subsequent transfer of the developed parameters to corresponding fragments of biological macromolecules.

Lennard-Jones parameters

Optimization of LJ parameters represents the most difficult aspect of empirical force field development as this term impacts the strength of ionic and hydrogen bond interactions as well as dispersion types of interactions. Adjustment of the LJ parameters was performed to reproduce experimental molecular volumes and enthalpies of vaporization of the neat alcohols, with the relative values of the LJ parameters checked via interactions with rare gases, as previously performed.[49] All alkyl groups were constrained to the previously determined alkane LJ values[27] and the polar hydrogen LJ parameters were constrained to a well depth of 0.01 kcal/mol and radius, $R_{min}/2$, of 0.4 Å. Such LJ parameters on the polar H introduce a repulsive potential on the hydrogen atom to diminish the possibility of overpolarization during hydrogen or ionic bonding interactions. Based on these assumptions only the oxygen LJ parameters were optimized subject to the constraint that the same oxygen LJ parameters were to be utilized throughout the alcohol series, with the only exception being the LJ parameters of the methyl group in methanol. This strategy was selected to facilitate parameter transferability to a biomacromolecular force field and to limit the overall number of atom types in the force field. However, such a limitation will diminish the quality of the fit for the individual alcohols, though the compromise to be made is moderate (see below). Final optimized values of the oxygen well depth and $R_{min}/2$ were 0.15 kcal/mol and 1.765 Å, respectively. The derived oxygen LJ parameters are relatively close to the polarizable SWM4-NDP water model LJ parameters where the well depth is 0.21 kcal/mol and $R_{min}/2$ is 1.79 Å. Additionally well depth parameters on the methyl carbon and hydrogen in methanol were optimized to obtain better agreement with the experimental molecular volume, which was otherwise too large. The LJ radii on the methyl atoms were constrained to the alkane values,[27] as condensed-phase properties of methanol were considerably less sensitive to changes in the LJ radii than in the well depths, ε. Final values of well depth for methanol were ε(C)=0.11 and ε(H)=0.035 kcal/mol. The Lennard-Jones parameters on other aliphatic C,H atoms were preserved at their alkane values.[27]

One of the common assumptions in empirical force fields is the use of combining or mixing rules to convert LJ parameters for individual atom types to those for atom pairs.[80–82] This assumption is largely for convenience avoiding the need to individually determine LJ terms for each atom type pair. However, in the present work it was observed that the LJ parameters of the hydroxyl oxygen that yielded good pure solvent condensed phase properties lead to both the interaction energies with individual water molecules as well as the free energies of aqueous solvation being too favorable. This motivated the use of a specific, or off-diagonal (ie. NBFIX), LJ term for the $O_{alcohol}\ldots O_{water}$ atom pairs, with individual terms for the primary and secondary hydroxyl oxygens. As shown above in Table 3 and Table 4 and presented below, this leads to good agreement for the aforementioned properties and will be part of the present alcohol force field.

Computed and experimental properties for the neat liquids are summarized in Table 8. Data were obtained for the training set molecules, methanol, ethanol and 2-propanol as well as for the test molecule 2-butanol, 1-propanol and 1-butanol. Overall, the level of agreement of the polarizable model is quite good, especially with methanol, ethanol, 2-propanol and 2-butanol. For all the compounds the molecular volumes are generally improved over CHARMM22, the

exception being 2-propanol. Concerning the heats of vaporization both the polarizable and additive models are good for methanol, ethanol and 2-propanol, with CHARMM22 significantly underestimating the value for 2-butanol while the polarizable model significantly underestimates the heats for 1-propanol and 1-butanol. Thus, it appears that neither of the models is capable of accurately reproducing pure solvent properties for the full series of primary and secondary alcohols. While this may be associated with constraints on the number of parameters optimized to assure transferability, similar problems have been observed in polarizable alcohol force fields based on both induced dipole and fluctuating charge models.[18, 21, 22] In the induced dipole model, the heats of vaporization were typically in good agreement with experiment while molecular volumes were overestimated for the smaller alcohols and underestimated for the larger compounds.[18] With the fluctuating charge force field distinct parameters were used for methanol[21] and ethanol[22] to obtain agreement with experiment. Thus, despite the inclusion of polarizability, it appears that the current form of the energy function, combined with limitations associated with the need to develop transferable parameters, is not capable of accurately treating the full series of primary and secondary alcohols.

A natural extension of the present parameterization will be to model longer aliphatic-chain alcohols. To this end, the development of LJ parameters for the oxygen targeting the 1-propanol and 1-butanol pure solvent properties was undertaken. This model only differed in those LJ parameters; the remainder of the force field was maintained. Results in Table 8 (the alternative LJ model) show the second LJ model to yield good agreement for 1-propanol and 1-butanol. This second model, with a well depth = 0.15 kcal/mol and $R_{min}/2$ = 1.74 Å on the alcohol oxygen, is recommended for use on long chain primary alcohols. Also included in Table 8 are results using that alternative LJ model for ethanol, 2-propanol and 2-butanol, for comparison with the original model. Basically, the utility of the alternative LJ set for hydroxyl oxygen is limited to long-chain primary alcohols only.

To minimize the impact of parameter correlation during the optimization of LJ parameters, interactions with rare gases were monitored to facilitate optimization of the relative values of the LJ parameters. The target data from the rare gas interactions were the RMS fluctuations about the average difference (or ratios) for the minimum interaction energies and distances. Use of this target data allows for the LJ parameters to produce interactions that are systematically offset from the QM data to indicate that the relative LJ parameters for different atom types are properly balanced while accounting for limitations in QM methods to treat dispersion interactions[49]. Shown in Table 9 are the RMS fluctuations for CHARMM22 and the final polarizable model for methanol and ethanol, with additional details supplied in Table S4 of the supporting information. The RMS values for the two models are similar, indicating that the polarizable model did not improve the balance of the LJ parameters using interactions with rare gases as a metric. Analysis of the individual minimum interaction distance differences shows those associated with direct interactions with the lone pairs (120 interaction) and hydroxyl hydrogen (ROH interaction, Figure 3) to be significantly shorter for the empirical models as compared to the target QM data. Such difference suggests that the empirical models may benefit from assignment of LJ parameters on lone-pair sites and the hydroxyl hydrogens. However, in the present model LJ parameters are not applied to the lone pairs for simplicity and a standard LJ parameter is applied to the polar hydrogen to facilitate transferability of the model.

Additional condensed phase properties of the alcohols

Additional properties of the pure solvents investigated include the dielectric constants, diffusion constants, isothermal compressibilities and structural features based on radial distribution functions. In addition, free energies of solvation of the final models were evaluated.

An important feature of a model is proper treatment of the dielectric constant as this term is important in dictating the energetics of dissolution of solutes in the alcohols. Dielectric constants for both the Drude and additive models as well as the experimental data are presented in Table 10. The additive model systematically underestimates the dielectric constant on an average percent difference of −35.9 %, an inherent limitation of the model due to the lack of explicit polarizability, as previously described for alkanes.[27] With the Drude model, larger dielectric constants are obtained, leading to systematically better agreement with experiment with an average percent difference of −2.3%. As the internal parameters in the additive and polarizable models are similar the improvement in description of dielectric constant is clearly due to the explicit description of electronic polarization. Small underestimations are observed for ethanol and 2-propanol, the results for methanol, 1-propanol and 2-butanol are quite good, whereas 1-butanol overestimates the experimental data. Computations of dielectric constant show that this is a very slow converging property. In the current study five independent condensed-phase runs of 5 ns were performed for each alcohol molecule yield a total of 25 ns of simulation time. Longer simulations may be beneficial to obtain more reliable estimates; however, the present results already illustrate the advantage of the polarizable model over the additive one.

Self-diffusion coefficients and isothermal compressibilities for four of the alcohols are presented in Table 11 and Table 12. Diffusion constant data include the values obtained directly from the periodic boundary simulations, a correction for PBC effects on the diffusion[63], and the total values along with the experimental values. The results demonstrate that the polarizable model to be an improvement over the additive one, although there is a tendency to slightly overestimate the experimental values. Concerning the isothermal compressibilities the calculated results show better agreement with the additive model for methanol and 2-propanol while the polarizable model is equivalent or better for ethanol and 1-propanol. Overall, there is a tendency for the polarizable model to underestimate the compressibilities, with the exception of ethanol at 343 K.

Radial distribution functions (RDF) for the methanol, ethanol, and 2-propanol were obtained to analyze structural features of those pure solvents. O-H and O-O radial distribution functions for these solvents along with coordination numbers as a function of distance are shown in Figure 6. Comparison of the polarizable and additive g(r)s show minor but systematic differences. In all cases the first peak is higher in the polarizable model, indicating a higher degree of structural organization. The peak is also shifted to shorter distances in the polarizable model. For example, the first peak in the O-H RDF shifts in from 1.87 to 1.81 Å upon going from the additive to the polarizable model for all studied alcohols. A similar shift from 2.81 to 2.75 Å occurs in the O-O RDFs. The computed RDFs of the O-O and O-H distances in ethanol are in satisfactory agreement with experimental data. Neutron scattering[83] and X-ray diffraction[84] show the first peak in the O-O RDF to occur in the range 2.7–2.8 Å. The calculated coordination numbers are 2.00 and 1.99 to the first minimum occurring at 3.54 and 3.61 Å in the O-O RDFs for the polarizable and additive model, respectively, which compare well with the experimental value of 2.0 reported at 3.0 Å, the location of the minimum in the experimental work. Empirical O-H coordination numbers out to the first minima integrate to 0.97 at 2.68 Å and 0.98 at 2.64 Å for additive and polarizable models, respectively. These are in good agreement with neutron scattering data for liquid ethanol where oxygen is surrounded by 0.95 hydroxyl atoms up to the first minima at 2.1 Å. Beyond the first peak the g(r)s are similar for the two solvents. Thus, upon going from the additive to the polarizable model there is a significant change in the O-O and O-H pair correlation function for ethanol and 2-propanol, although the second peaks and the coordination numbers are similar for the two models.

While the optimization process was dominated by the pure solvent properties, free energies of aqueous solvation values were also considered during the optimization, though their weight in

the selection of the final parameter set was less than that assigned to the pure solvents. Table 13 shows the additive, Drude and experimental free energies of solvation for the alcohols studied; the free energies include a long-range correction (LRC) for the truncation of the LJ atom-atom interactions. The CHARMM22 results are in good agreement with experiment, though they tend to be too favorable than the experimental data by 4 to 19 percent. In the polarizable model this tendency was enhanced when LJ parameters based on the pure solvent simulations were used (see Table 13, ΔG_{uncorr}), with the largest percent difference being 34 % for 2-butanol (Table S5 of the supplemental information). To overcome this trend atom type $O_{alcohol}$-O_{water} LJ terms were developed. These terms lead to improved agreement for the interactions of the alcohols with water (Table 3 and Table 4) and for the free energies of solvation (Table 13). During this process it was observed that the $O_{alcohol}$-O_{water} LJ term developed based on ethanol led to the ΔG_{solv} values still too favorable for the secondary alcohols by −0.5 to −0.6 kcal/mol (not shown). Therefore, a secondary alcohol specific $O_{alcohol}$…O_{water} LJ term was optimized, yielding the results shown in Table 3, Table 4 and Table 13. The resulting pair specific $O_{alcohol}$…O_{water} LJ terms were (ε_{ij}=0.18 kcal/mol; R_{min_ij}=3.58 Å for the primary alcohols and ε_{ij}=0.21 kcal/mol; R_{min_ij}=3.60 Å for the secondary alcohols) replacing the corresponding terms (ε_{ij}=0.17788 kcal/mol; R_{min_ij}=3.5519 Å for both primary and secondary alcohols) generated by the combining rule. While the use of a specific $O_{alcohol}$-O_{water} LJ terms for the primary and secondary alcohols deviates from the goal of a fully transferable alcohol model, the significant improvement in the aqueous solvation warrants this decision.

With respect to previous studies ΔG_{solv} values of −4.88 and −4.08 kcal/mol for methanol and ethanol, respectively, were obtained by Deng and Roux for the CHARMM22 force field using a spherical solvent boundary potential (SSBP).[66] Pande and coworkers[85] used periodic boundary conditions (PBC) simulations with thermodynamic integration along with extensive sampling (with 5 ns per window versus 100 ps in the present work) to obtain free energies of solvation of −4.59 and −4.22 kcal/mol for the CHARMM22 methanol and ethanol models, respectively. Comparison with the CHARMM22 additive results shows the present results to be more favorable than the published values by 0.4 to 1.1 kcal/mol. Further analyses indicate that the variations are associated with methodological differences. The present computations were done using PBC with 250 water molecules, atom-based truncation, LJ switch truncation from 10 to 12 Å, treatment of long range electrostatic interactions via PME. The computations of Deng and Roux were done using 100 water molecules, LJ switch truncation from 10 to 12 Å, treatment of long range electrostatics with extended electrostatics and the SSBP continuum model. The computations of Pande and coworkers used PBC with 900 water molecules, group-based truncation, treatment of both LJ and electrostatic interactions with switch truncation over 10 to 12 Å (i.e. no long range electrostatic correction). These results emphasize the sensitivity of free energy perturbation calculations to differences in computational methodology.

Beyond methodological difference, the impact of the conformation of the alcohol on the obtained ΔG_{solv} was considered. This was performed by calculating the free energy of solvation of ethanol with the hydroxyl in either the gauche (60°) or trans (180°) conformation via inclusion of a harmonic restraint on the C-C-O-H dihedral of 1000 kcal/mol/rad^2. The resulting ΔG_{solv} values for the gauche and trans states, assuming the same LRC corrections reported in Table 13, were −5.01 and −5.61 kcal/mol, respectively, for CHARMM22 and −4.48 and −5.52 kcal/mol, respectively, for the Drude model. Thus, the relative g versus t conformations may lead to significant differences in the obtained free energy of solvation. While ethanol stayed in the trans conformation in the present study, with the same behavior presumably occurring in the studies discussed in the preceding paragraph, the potential impact of the conformation of the hydroxyl should be noted.

It is interesting to note that the observed trends in hydration free energies of ethanol as a function of conformation is opposite to the gas-phase dipole moments of polarizable ethanol (μ_{gauche}=1.96 D, μ_{trans}=1.81 D). Such a difference indicates that the relative free energy of solvation of ethanol is dictated by the higher degree of availability of the hydroxyl group in the trans-conformation to intermolecular hydrogen bonds rather than the intrinsic dipole moment. This speaks to the importance of the proper treatment of intermolecular interactions in the gas versus condensed phases, including proper polarization contribution, and their impact on condensed phase properties.

RDFs of water with ethanol and 2-propanol were analyzed to check the impact of the polarizable model on structural properties in solution with respect to CHARMM22. Analysis of Figure 7 shows there to be significant difference between the polarizable and additive force fields. In the $O_{alcohol}$-H_{water} RDFs the polarizable model has the first peak shifted to longer values versus the additive model while the opposite is true for the $H_{alcohol}$-O_{water} RDF. In addition, with the $O_{alcohol}$-H_{water} RDF there are differences in the first minimum as well as the second peak. With the secondary alcohol, 2-propanol, even larger differences between the additive and polarizable models are observed, with the largest change in the $H_{alcohol}$-O_{water} RDF followed by the $O_{alcohol}$-O_{water} RDF. Thus, significant differences in the atomic details of the additive versus polarizable models are observed for in aqueous solution.

Explicit inclusion of electronic polarizability is anticipated to allow for more accurate modeling as a function of the polarity of the environment. To see if such effects occur in the Drude polarizable force field dipole distributions were obtained from MD simulations in the gas phase, the pure solvent and in aqueous solution for both the additive and polarizable models (Figure 8). Analysis of the figures shows extreme differences. The additive model has the three distributions clustered together with the maximum close to 2.4 D for both ethanol and 2-propanol. Such similar distributions are expected due to the lack of explicit polarizability, with the value of 2.4 being significantly larger than the gas phase experimental value for both molecules, as required to implicitly overpolarize the molecule to obtain reasonable condensed phase properties. With the polarizable model, significant differences are seen as a function of environment. From the MD simulations in the gas phase, which may be considered a hydrophobic environment, the distribution is centered around the gas phase experimental values (Table 7). Upon going to the pure solvent an upshift in the distribution which is centered around 2.4 and 2.5 D for ethanol and 2-propanol, respectively. Upon moving to the more polar aqueous environments additional upshifting occurs, where the distributions are now centered around 2.7 and 2.9 D for ethanol and 2-propanol, respectively. The value for ethanol is in good agreement with a Car-Parrinello MD prediction of the dipole moment of ethanol of 3.1 D for ethanol solvated in water.[86] Interestingly, the implicitly overpolarized additive model has a distribution similar to that of the polarizable model in the pure solvent, consistent with the satisfactory agreement for ΔH_{vap} for both models.

Further comparison of the dipole moment distributions were obtained from 500 ps MD simulation of ethanol in a box of 128 benzene molecules. The simulation using the polarizable model yields an average ethanol dipole moment of 1.86 D, close to the gas-phase value, while the additive model yields a value of 2.34 D. This result suggests that a model where polarizability changes as a function of environment has a distinct advantage over the fixed charge additive model.

Also of interest is the impact of the presence of the alcohol on the electrostatic properties of the surrounding water molecules. This was analyzed by calculating the average dipole moment of water molecules as a function of $O_{alcohol}$-O_{water} distance for ethanol in water (Figure 9). While the overall change in the dipole moment is 0.2 D, there is a clear trend for the water dipole moment to decrease from the bulk value in the vicinity of the first minimum in the

$O_{alcohol}$-O_{water} RDF followed by an increase upon moving in to shorter distance. The overall trends in the average dipole moment of water molecules interacting with ethanol as H-bond donors or acceptors are similar, though minor differences are present. It is observed that the variations in the total dipole of water molecules relax back to the average bulk value only after the second hydration shell (4–5 Å away from the solute). Incorporating such subtle effects clearly requires going beyond the mean field picture provided by effective additive force fields, in which all the water molecules are modeled with the same electrostatic charge distribution. These results further indicate the power of a polarizable model for the investigation of condensed phase properties.

Conclusions

An empirical polarizable force field for the alcohol series has been developed. Explicit incorporation of electronic polarizability via the classical Drude oscillator facilitates more realistic response of the model compounds to the degree of polarity of the environment, with the molecular dipole changing significantly upon transition from hydrophobic to hydrophilic environments. This represents a considerable improvement over the additive model of alcohols, indicating the polarizable model to yield a better balance of the types of interactions dictating structural and thermodynamic properties of condensed phases. Significant improvement is obtained in prediction of dielectric susceptibility of liquid alcohols due to the explicit incorporation of electronic polarizability. Notable improvement over the additive model in the prediction of self-diffusivity of alcohols is also obtained. The potential energy profiles for rotation about selected bonds show the Drude model to accurately reproduce the high-level QM correlated energy maps. The Drude model is in good agreement with experiment for both pure solvent and aqueous solvation properties, though the agreement with the free energies of solvation required the use of atom type specific terms for the $O_{alcohol}$-O_{water} LJ interactions, including individual terms for the primary and secondary alcohols. This represents a departure of the goal of transferability where the LJ parameters for the hydroxyls are identical in all the molecules and the LJ parameters for the aliphatic moieties were transferred directly from the alkanes.[27] In contrast, transferable LJ parameters were used in the additive model yielding a level of agreement with experiment typically better than that for the Drude model before the use of the atom type specific LJ terms. This poorer agreement is suggested to be due to additional sensitivity of the polarizable model to changes in the polarity of its environment leading to the constraint of transferability having a more adverse impact on that model versus than on the additive model, where the fixed-charge model diminishes the sensitivity of the model to the environment (including changes in the neighboring atoms forming the intramolecular “environment” of a given atom type). Supporting this are results from previously published polarizable models of alcohols were it was observed that the same LJ parameters could not be used for methanol and ethanol to yield agreement with experiment[18, 21, 22] and in a second study on a polarizable alcohol series where constraining the LJ parameters on the hydroxyl to be identical lead to a systematic variation of the pure solvent molecular volumes with respect to experiment.[18] Addressing this issue will be beneficial in gaining an understanding about effective ways to improve the predictive potential of empirical force fields.

Supplementary Material

Refer to Web version on PubMed Central for supplementary material.

Acknowledgement

Financial support for the work was received from the NIH (GM51501 and GM72558) and computational support was obtained from the DOD ACS Major Shared Resource Computing and PSC Pittsburgh Supercomputing Center.

References

1. Wensink EJW, Hoffmann AC, Maaren PJv, Spoel Dvd. Dynamic properties of water/alcohol mixtures studied by computer simulation. J. Chem. Phys 2003;119:7308–7317.
2. Jorgensen WL. Optimized intermolecular potential functions for liquid alcohols. J. Phys. Chem 1986;90:1276–1284.
3. Allinger NL, Chen K-H, Lii J-H, Durkin KA. Alcohols, ethers, carbohydrates, and related compounds. I. The MM4 force field for simple compounds. J. Comp. Chem 2003;24:1447–1472. [PubMed: 12868110]
4. Jorgensen WL, Maxwell DS, Tirado-Rives J. Development and Testing of the OPLS All-Atom Force Field on Conformational Energetics. J. Am. Chem. Soc 1996;118:11225–11236.
5. González MA, Bermejo FJ, Enciso E, Cabrillo C. Hydrogen bonding in condensed-phase alcohols: some keys to understanding their structure and dynamics. Philosophical Magazine 2004;84:1599–1607.
6. Taylor RS, Shields RL. Molecular-dynamics simulations of the ethanol liquid-vapor interface. J. Chem. Phys 2003;119:12569–12576.
7. Saiz L, Padro JA, Guardia E. Structure and Dynamics of Liquid Ethanol. J. Phys. Chem. B 1997;101:78–86.
8. Noskov SY, Kiselev MG, Kolker AM, Rode BM. Structure of methanol-methanol associates in dilute methanol-water mixtures from molecular dynamics simulation. J. Mol. Liq 2001;91:157–165.
9. Kiselev M, Ivlev D. The study of hydrophobicity in water–methanol and water–tert-butanol mixtures. J. Mol. Liq 2004;110:193–199.
10. Brooks BR, Bruccoleri RE, Olafson BD, States DJ, Swaminathan S, Karplus M. CHARMM: A program for macromolecular energy minimization and dynamics calculations. J. Comp. Chem 1983;4:187–217.
11. MacKerell AD, Bashford D, Bellott M, Dunbrack RL, Evanseck JD, Field MJ, Fischer S, Gao J, Guo H, Ha S, Joseph-McCarthy D, Kuchnir L, Kuczera K, Lau FTK, Mattos C, Michnick S, Ngo T, Nguyen DT, Prodhom B, Reiher WE, Roux B, Schlenkrich M, Smith JC, Stote R, Straub J, Watanabe M, Wiorkiewicz-Kuczera J, Yin D, Karplus M. All-Atom Empirical Potential for Molecular Modeling and Dynamics Studies of Proteins. J. Phys. Chem. B 1998;102:3586–3616.
12. Cornell WD, Cieplak P, Bayly CI, Gould IR, Merz KM, Ferguson DM, Spellmeyer DC, Fox T, Caldwell JW, Kollman PA. A Second Generation Force Field for the Simulation of Proteins, Nucleic Acids, and Organic Molecules. J. Am. Chem. Soc 1995;117:5179–5197.
13. Jorgensen WL, Tirado-Rives J. The OPLS [optimized potentials for liquid simulations] potential functions for proteins, energy minimizations for crystals of cyclic peptides and crambin. J. Am. Chem. Soc 1988;110:1657–1666.
14. Halgren TA. MMFF VII. Characterization of MMFF94, MMFF94s, and other widely available force fields for conformational energies and for intermolecular-interaction energies and geometries. J. Comp. Chem 1999;20:730–748.
15. Mayo SL, Olafson BD, Goddard WA. DREIDING: a generic force field for molecular simulations. J. Phys. Chem 1990;94:8897–8909.
16. Caldwell JW, Kollman PA. Structure and Properties of Neat Liquids Using Nonadditive Molecular Dynamics: Water, Methanol, and N-Methylacetamide. J. Phys. Chem 1995;99:6208–6219.
17. Wang J, Cieplak P, Kollman PA. How well does a restrained electrostatic potential (RESP) model perform in calculating conformational energies of organic and biological molecules? J. Comp. Chem 2000;21:1049–1074.
18. Gao J, Habibollazadeh D, Shao L. A Polarizable Intermolecular Potential Function for Simulation of Liquid Alcohols. J. Phys. Chem 1995;99:16460–16467.
19. Noskov SY, Lamoureux G, Roux B. Molecular Dynamics Study of Hydration in Ethanol - Water Mixtures Using a Polarizable Force Field. J. Phys. Chem. B 2005;109:6705–6713. [PubMed: 16851754]
20. Kaminski GA, Stern HA, Berne BJ, Friesner RA. Development of an Accurate and Robust Polarizable Molecular Mechanics Force Field from ab Initio Quantum Chemistry. J. Phys. Chem. A 2004;108:621–627.

21. Patel S, Brooks CL III. A nonadditive methanol force field: Bulk liquid and liquid-vapor interfacial properties via molecular dynamics simulations using a fluctuating charge model. J. Chem. Phys 2003;122:1–10.024508
22. Patel S, Brooks CL III. Structure, thermodynamics, and liquid-vapor equilibrium of ethanol from molecular-dynamics simulations using nonadditive interactions. J. Chem. Phys 2005;123:1–12.164502
23. Yu H, Geerke DP, Liu H, Gunsteren WFv. Molecular dynamics simulations of liquid methanol and methanol-water mixtures with polarizable models. J. Comp. Chem 2006;27:1494–1504. [PubMed: 16838298]
24. Dang LX, Chang T-M. Many-body interactions in liquid methanol and its liquid/vapor interface: A molecular dynamics study. J. Chem. Phys 2003;119:9851–9857.
25. Lamoureux G, MacKerell AD Jr, Roux B. A simple polarizable model of water based on classical Drude oscillators. J. Chem. Phys 2003;119:5185–5197.
26. Lamoureux GH, Edward, Vorobyov IV, Roux B, MacKerell JAD. A polarizable model of water for molecular dynamics simulations of biomolecules. Chem. Phys. Lett 2006;418:245–249.
27. Vorobyov IV, Anisimov VM, MacKerell ADJ. Polarizable Empirical Force Field for Alkanes Based on the Classical Drude Oscillator Model. J. Phys. Chem. B 2005;109:18988–18999. [PubMed: 16853445]
28. Lopes PEM, Lamoureux G, Roux B, MacKerell AD Jr. Polarizable Empirical Force Field for Aromatic Compounds Based on the Classical Drude Oscillator. J. Phys. Chem. B. 2007
29. Vorobyov I, Anisimov VM, Greene S, Venable RM, Moser A, Pastor RW, MacKerell AD Jr. Additive and Classical Drude Polarizable Force Field for Linear and Cyclic Ethers. J. Chem. Theory Comput. 2007
30. Lamoureux G, Roux B. Modeling induced polarization with classical Drude oscillators: Theory and molecular dynamics simulation algorithm. J. Chem. Phys 2003;119:3025–3039.
31. Iftimie R, Minary P, Tuckerman ME. Ab initio molecular dynamics: Concepts, recent developments, and future trends. PNAS 2005;102:6654–6659. [PubMed: 15870204]
32. MacKerell AD Jr. Empirical force fields for biological macromolecules: Overview and issues. J. Comp. Chem 2004;25:1584–1604. [PubMed: 15264253]
33. Harder E, Anisimov VM, Vorobyov IV, Lopes PEM, Noskov SY, MacKerell AD Jr, Roux B. Atomic Level Anisotropy in the Electrostatic Modeling of Lone Pairs for a Polarizable Force Field Based on the Classical Drude Oscillator. J. Chem. Theory Comput 2006;2:1587–1597.
34. Thole BT. Molecular polarizabilities calculated with a modified dipole interaction. Chem. Phys 1981;59:341–350.
35. van Duijnen PT, Swart M. Molecular and Atomic Polarizabilities: Thole's Model Revisited. J. Phys. Chem. A 1998;102:2399–2407.
36. Anisimov VM, Lamoureux G, Vorobyov IV, Huang N, Roux B, MacKerell AD Jr. Determination of Electrostatic Parameters for a Polarizable Force Field Based on the Classical Drude Oscillator. J. Chem. Theory Comput 2005;1:153–168.
37. Miller KJ. Additivity methods in molecular polarizability. J. Am. Chem. Soc 1990;112:8533–8542.
38. Head-Gordon M, Pople JA, Frisch MJ. MP2 energy evaluation by direct methods. Chem. Phys. Letters 1988;153:503–506.
39. Frisch, MJ.; Trucks, GW.; Schlegel, HB.; Scuseria, GE.; Robb, MA.; Cheeseman, JR.; Montgomery, JJA.; Vreven, T.; Kudin, KN.; Burant, JC.; Millam, JM.; Iyengar, SS.; Tomasi, J.; Barone, V.; Mennucci, B.; Cossi, M.; Scalmani, G.; Rega, N.; Petersson, GA.; Nakatsuji, H.; Hada, M.; Ehara, M.; Toyota, K.; Fukuda, R.; Hasegawa, J.; Ishida, M.; Nakajima, T.; Honda, Y.; Kitao, O.; Nakai, H.; Klene, M.; Li, X.; Knox, JE.; Hratchian, HP.; Cross, JB.; Bakken, V.; Adamo, C.; Jaramillo, J.; Gomperts, R.; Stratmann, RE.; Yazyev, O.; Austin, AJ.; Cammi, R.; Pomelli, C.; Ochterski, JW.; Ayala, PY.; Morokuma, K.; Voth, GA.; Salvador, P.; Dannenberg, JJ.; Zakrzewski, VG.; Dapprich, S.; Daniels, AD.; Strain, MC.; Farkas, O.; Malick, DK.; Rabuck, AD.; Raghavachari, K.; Foresman, JB.; Ortiz, JV.; Cui, Q.; Baboul, AG.; Clifford, S.; Cioslowski, J.; Stefanov, BB.; Liu, G.; Liashenko, A.; Piskorz, P.; Komaromi, I.; Martin, RL.; Fox, DJ.; Keith, T.; Al-Laham, MA.; Peng, CY.; Nanayakkara, A.; Challacombe, M.; Gill, PMW.; Johnson, B.; Chen, W.; Wong, MW.; Gonzalez, C.; Pople, JA. Gaussian 03, Revision C.02. Wallingford CT: Gaussian, Inc.; 2004.

40. Becke AD. Density-functional exchange-energy approximation with correct asymptotic behavior. Phys. Rev. A 1988;38:3098–3100. [PubMed: 9900728]
41. Lee C, Yang W, Parr RG. Development of the Colle-Salvetti correlation-energy formula into a functional of the electron density. Phys. Rev. B 1988;37:785–789.
42. Becke AD. Density-functional thermochemistry. III. The role of exact exchange. J. Chem. Phys 1993;98:5648–5652.
43. Vosko SH, Wilk L, Nusair M. Accurate spin-dependent electron liquid correlation energies for local spin density calculations: a critical analysis. Can. J. Phys 1980;58:1200–1211.
44. Stephens PJ, Devlin FJ, Chabalowski CF, Frisch MJ. Ab Initio Calculation of Vibrational Absorption and Circular Dichroism Spectra Using Density Functional Force Fields. J. Phys. Chem 1994;98:11623–11627.
45. Kendall RA, Dunning TH Jr, Harrison RJ. Electron affinities of the first-row atoms revisited. Systematic basis sets and wave functions. J. Chem. Phys 1992;96:6796–6806.
46. Saebo S, Pulay P. Local Treatment of Electron Correlation. Annu. Rev. Phys. Chem 1993;44:213–236.
47. Murphy RB, Beachy MD, Friesner RA, Ringnalda MN. Pseudospectral localized Møller–Plesset methods: Theory and calculation of conformational energies. J. Chem. Phys 1995;103:1481–1490.
48. Huang N, MacKerell AD Jr. An ab Initio Quantum Mechanical Study of Hydrogen-Bonded Complexes of Biological Interest. J. Phys. Chem. A 2002;106:7820–7827.
49. Yin D, MacKerell AD Jr. Combined ab initio/empirical approach for optimization of Lennard-Jones parameters. J. Comp. Chem 1998;19:334–348.
50. Chu J-W, Trout BL, Brooks BR. A super-linear minimization scheme for the nudged elastic band method. J. Chem. Phys 2003;119:12708–12717.
51. Allen FH. The Cambridge Structural Database: a quarter of a million crystal structures and rising. Acta Cryst. B 2002;58:370–379. [PubMed: 12037358]
52. Scott AP, Radom L. Harmonic Vibrational Frequencies: An Evaluation of Hartree-Fock, Mller-Plesset, Quadratic Configuration Interaction, Density Functional Theory, and Semiempirical Scale Factors. J. Phys. Chem 1996;100:16502–16513.
53. Kuczera K, Wiorkiewicz-Kuczera J. MOLVIB program. 1991
54. Pulay P, Fogarasi G, Pang F, Boggs JE. Systematic ab initio gradient calculation of molecular geometries, force constants, and dipole moment derivatives. J. Am. Chem. Soc 1979;101:2550–2560.
55. Dunning THJ. Gaussian basis sets for use in correlated molecular calculations. I. The atoms boron through neon and hydrogen. J. Chem. Phys 1989;90:1007–1023.
56. Evans DJ, Holian BL. The Nose–Hoover thermostat. J. Chem. Phys 1985;83:4069–4074.
57. Andersen HC. Molecular dynamics simulations at constant pressure and/or temperature. J. Chem. Phys 1980;72:2384–2393.
58. Ryckaert J-P, Ciccotti G, Berendsen HJC. Numerical integration of the cartesian equations of motion of a system with constraints: molecular dynamics of *n*-alkanes. J. Comp. Phys 1977;23:327–341.
59. Steinbach PJ, Brooks BR. New spherical-cutoff methods for long-range forces in macromolecular simulation. J. Comp. Chem 1994;15:667–683.
60. Allen, MP.; Tildesley, DJ. Computer Simulation of Liquids. Oxford, UK: Clarendon Press; 1987.
61. Darden TA, York DM, Pedersen LG. Particle mesh Ewald: An N·log(N) method for Ewald sums in large systems. J. Chem. Phys 1993;98:10089–10092.
62. Klauda JB, Brooks BR, MacKerell AD Jr, Venable RM, Pastor RW. An ab Initio Study on the Torsional Surface of Alkanes and Its Effect on Molecular Simulations of Alkanes and a DPPC Bilayer. J. Phys. Chem. B 2005;109:5300–5311. [PubMed: 16863197]
63. Yeh IC, Hummer G. System-Size Dependence of Diffusion Coefficients and Viscosities from Molecular Dynamics Simulations with Periodic Boundary Conditions. J. Phys. Chem. B 2004;108:15873–15879.
64. Simonson, T. Free Energy Calculations. In: Becker, OM.; MacKerell, AD., Jr; Roux, B.; Watanabe, M., editors. Computational Biochemistry and Biophysics. New York: Marcel Dekker; 2001. p. 169
65. Kollman PA. Free energy calculations: Applications to chemical and biochemical phenomena. Chem. Rev 1993;93:2395–2417.

66. Deng Y, Roux B. Hydration of Amino Acid Side Chains: Nonpolar and Electrostatic Contributions Calculated from Staged Molecular Dynamics Free Energy Simulations with Explicit Water Molecules. J. Phys. Chem. B 2004;108:16567–16576.

67. Weeks JD, Chandler D, Andersen HC. Role of Repulsive Forces in Determining the Equilibrium Structure of Simple Liquids. J. Chem. Phys 1971;54:5237–5247.

68. Kumar S, Rosenberg JM, Bouzida D, Swendsen RH, Kollman PA. The weighted histogram analysis method for free-energy calculations on biomolecules. I. The method. J. Comp. Chem 1992;13:1011–1021.

69. Straatsma TP, Berendsen HJC, Postma JPM. Free energy of hydrophobic hydration: A molecular dynamics study of noble gases in water. J. Chem. Phys 1986;85:6720–6727.

70. Pearlman DA. A Comparison of Alternative Approaches to Free Energy Calculations. J. Phys. Chem 1994;98:1487–1493.

71. Pearlman DA. Free energy derivatives: A new method for probing the convergence problem in free energy calculations. J. Comp. Chem 1994;15:105–123.

72. Jorgensen WL, Chandrasekhar J, Madura JD, Impey RW, Klein ML. Comparison of simple potential functions for simulating liquid water. J. Chem. Phys 1983;79:926–935.

73. Neumann M, Steinhauser O. Computer simulation and the dielectric constant of polarizable polar systems. Chem. Phys. Letters 1984;106:563–569.

74. Bayly CI, Cieplak P, Cornell W, Kollman PA. A well-behaved electrostatic potential based method using charge restraints for deriving atomic charges: the RESP model. J. Phys. Chem 1993;97:10269–10280.

75. Foloppe N, MacKerell AD Jr. All-atom empirical force field for nucleic acids: I. Parameter optimization based on small molecule and condensed phase macromolecular target data. J. Comp. Chem 2000;21:86–104.

76. Dixon RW, Kollman PA. Advancing beyond the atom-centered model in additive and nonadditive molecular mechanics. J. Comp. Chem 1997;18:1632–1646.

77. Yu H, Gunsteren WFv. Accounting for polarization in molecular simulation. Comput. Phys. Commun 2005;172:69–85.

78. Harder E, Kim B, Friesner RA, Berne BJ. Efficient Simulation Method for Polarizable Protein Force Fields: Application to the Simulation of BPTI in Liquid Water. J. Chem. Theory Comput 2005;1:169–180.

79. Patel S, Mackerell AD Jr, Brooks CL III. CHARMM fluctuating charge force field for proteins: II Protein/solvent properties from molecular dynamics simulations using a nonadditive electrostatic model. J. Comp. Chem 2004;25:1504–1514. [PubMed: 15224394]

80. Halgren TA. The representation of van der Waals (vdW) interactions in molecular mechanics force fields: potential form, combination rules, and vdW parameters. J. Am. Chem. Soc 1992;114:7827–7843.

81. Waldman M, Hagler AT. New combining rules for rare gas van der waals parameters. J. Comp. Chem 1993;14:1077–1084.

82. Al-Matar AK, Rockstraw DA. A generating equation for mixing rules and two new mixing rules for interatomic potential energy parameters. J. Comp. Chem 2004;25:660–668. [PubMed: 14978709]

83. Benmore CJ, Loh YL. The structure of liquid ethanol: A neutron diffraction and molecular dynamics study. J. Chem. Phys 2000;112:5877–5883.

84. Narten AH, Habenschuss A. Hydrogen bonding in liquid methanol and ethanol determined by x-ray diffraction. J. Chem. Phys 1984;80:3387–3391.

85. Shirts MR, Pitera JW, Swope WC, Pande VS. Extremely precise free energy calculations of amino acid side chain analogs: Comparison of common molecular mechanics force fields for proteins. J. Chem. Phys 2003;119:5740–5761.

86. Erp, TSv; Meijer, EJ. Ab initio molecular dynamics study of aqueous solvation of ethanol and ethylene. J. Chem. Phys 2003;118:8831–8840.

87. Lide, DR. CRC Handbook of Chemistry and Physics. 84th ed.. CRC Press; 2003. p. 2616

88. Karger N, Vardag T, Lüdemann H-D. Temperature dependence of self-diffusion in compressed monohydric alcohols. J. Chem. Phys 1990;93:3437–3444.

89. Yu Y-X, Gao G-H. Study on self-diffusion in water, alcohols and hydrogen fluoride by the statistical associating fluid theory. Fluid Phase Equilibria 2001;179:165–179.

90. Partington JR, Hudson RF, Bagnall KW. Self-diffusion of Aliphatic Alcohols. Nature 1952;169:583–584.

91. Meckl S, Zeidler MD. Self-diffusion measurements of ethanol and propanol. Mol. Phys 1988;63:85–95.

92. Kelly CP, Cramer CJ, Truhlar DG. SM6: A Density Functional Theory Continuum Solvation Model for Calculating Aqueous Solvation Free Energies of Neutrals, Ions, and Solute-Water Clusters. J. Chem. Theory Comput 2005;1:1133–1152.

93. Ooi T, Oobatake M, Nemethy G, Scheraga HA. Accessible Surface Areas as a Measure of the Thermodynamic Parameters of Hydration of Peptides. PNAS 1987;84:3086–3090. [PubMed: 3472198]

94. Coussan S, Bouteiller Y, Perchard JP, Zheng WQ. Rotational Isomerism of Ethanol and Matrix Isolation Infrared Spectroscopy. J. Phys. Chem. A 1998;102:5789–5793.

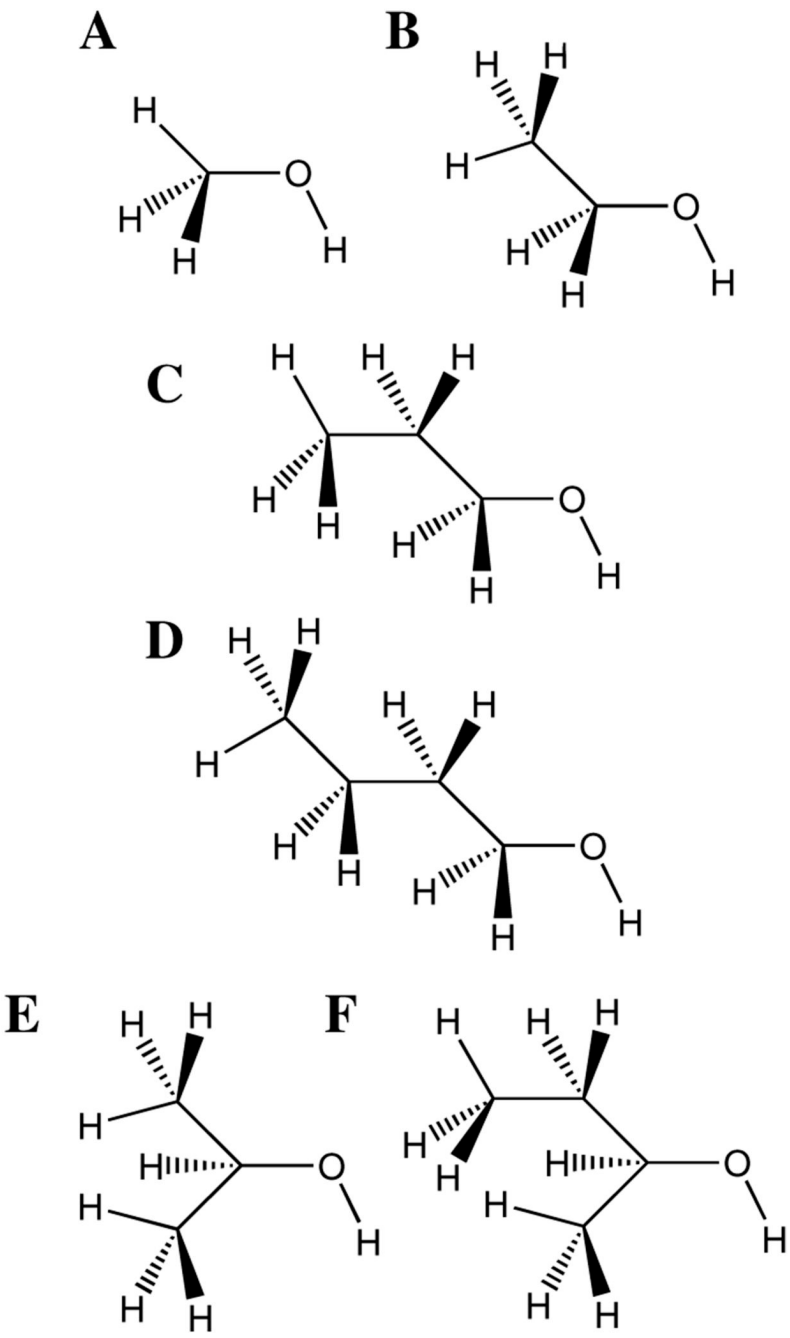

Figure 1.
Model compounds used in the parameter optimization. Primary alcohols A) methanol, B) ethanol, C) 1-propanol and D) 1-butanol and secondary alcohols E) 2-propanol (isopropanol) and F) 2-butanol.

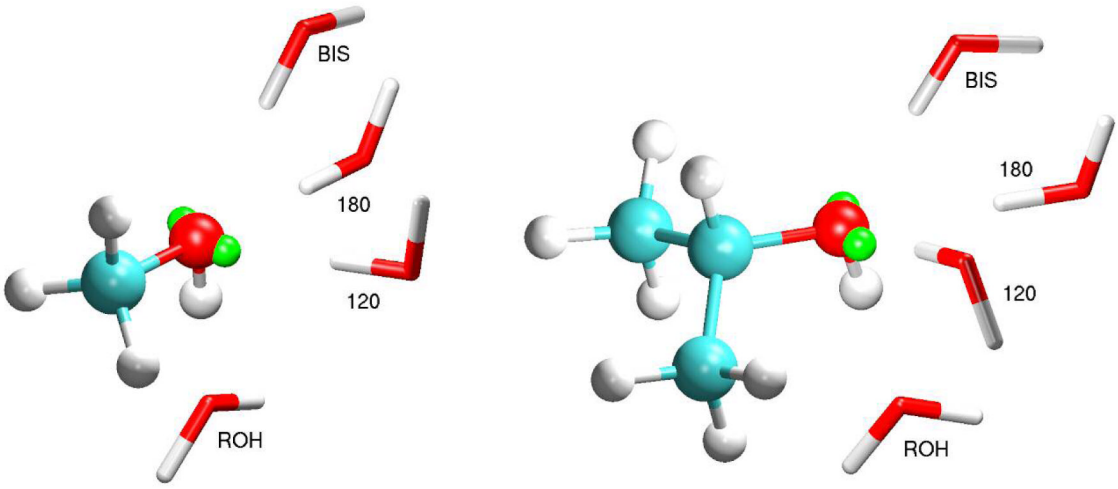

Figure 2.

Interaction orientations between water and the alcohols using methanol (left) and 2-propanol (right) as examples. Lone-pair sites are shown in green. BIS-orientation C-O-Hw angle is 115.8, 117.4, and 117.2° for methanol, ethanol, and isopropanol, respectively; 120-orientation C-O-Hw angle is 104.4, 108.3, and 105.1°, respectively; 120-orientation H(O)-C-O-Hw torsion is 108.0, 131.3, and 118.0°, respectively.

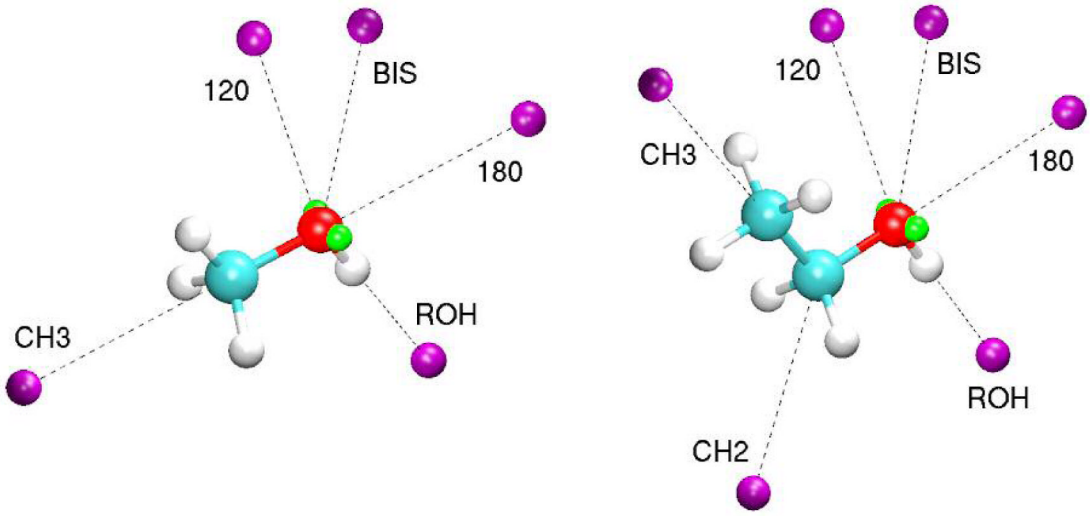

Figure 3.
Interaction orientation of the rare gases with the alcohols methanol (left) and ethanol (right). Rare-gas atoms are shown in purple and lone-pair sites are shown in green.

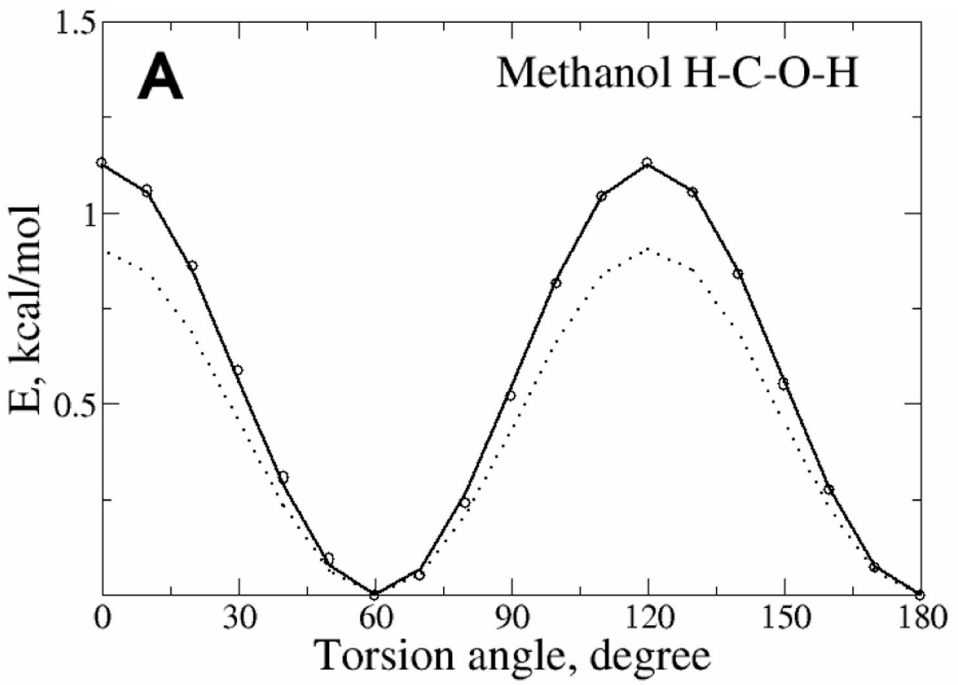

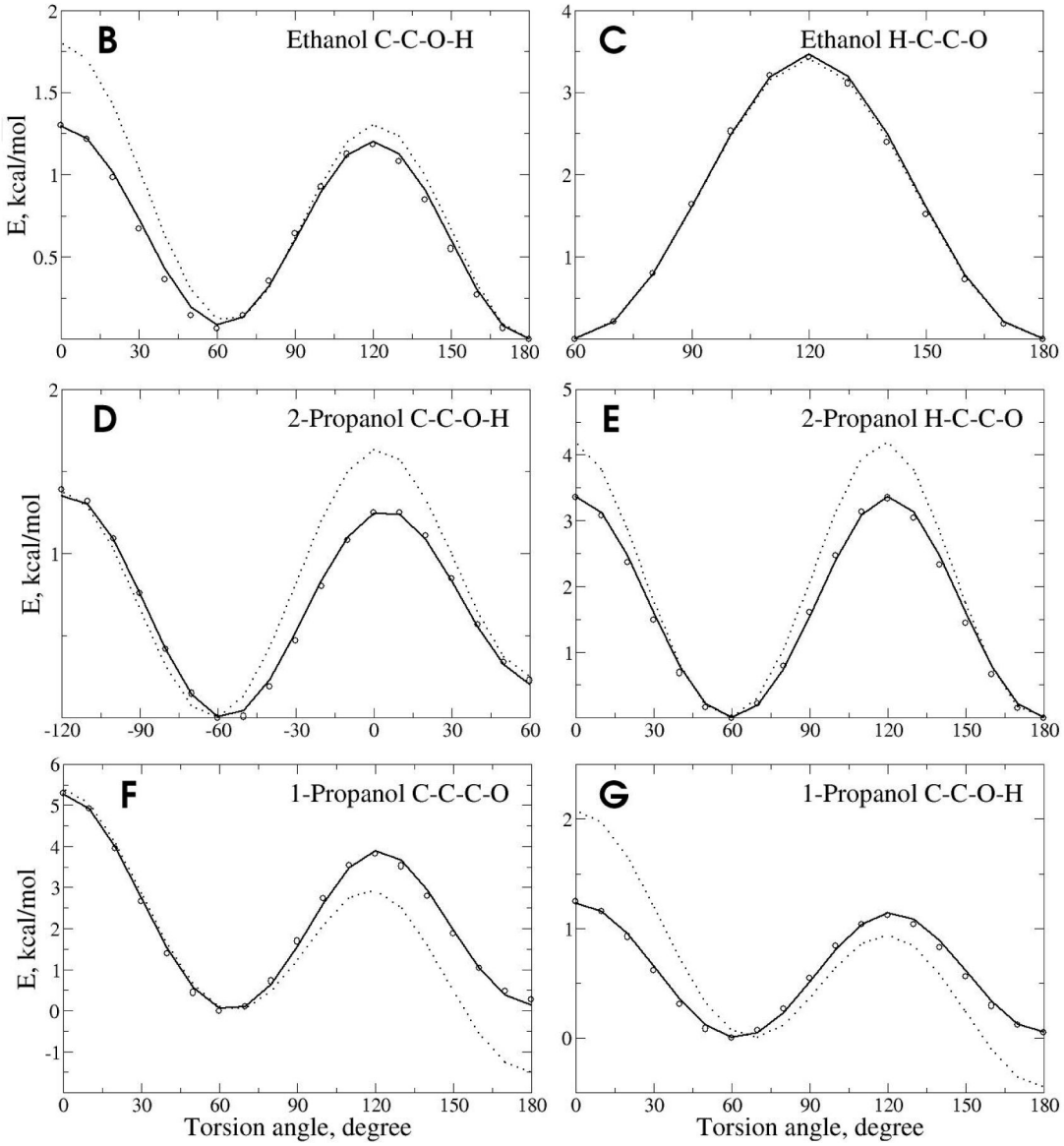

Figure 4.

Potential energy surfaces for rotation of selected dihedrals in methanol (A), ethanol (B and C), 1-propanol (D and E) and 2-propanol (F and G). Data is included from the QM (circles), Drude (solid line) and CHARMM22 (dotted line) models.

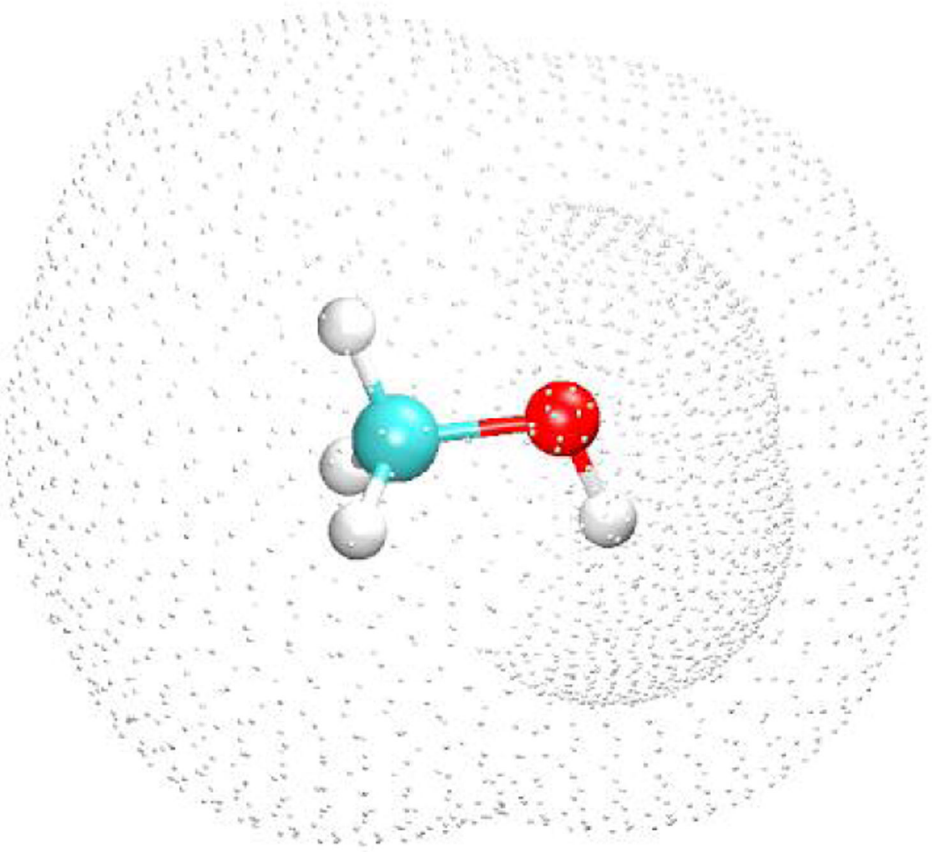

Figure 5.
Image of the additional Connolly surfaces around methanol at vdW scale factors of 1.3 and 2.2. See Table 1 for details of all grid surfaces and perturbation ion positions used in the electrostatic parameter fitting.

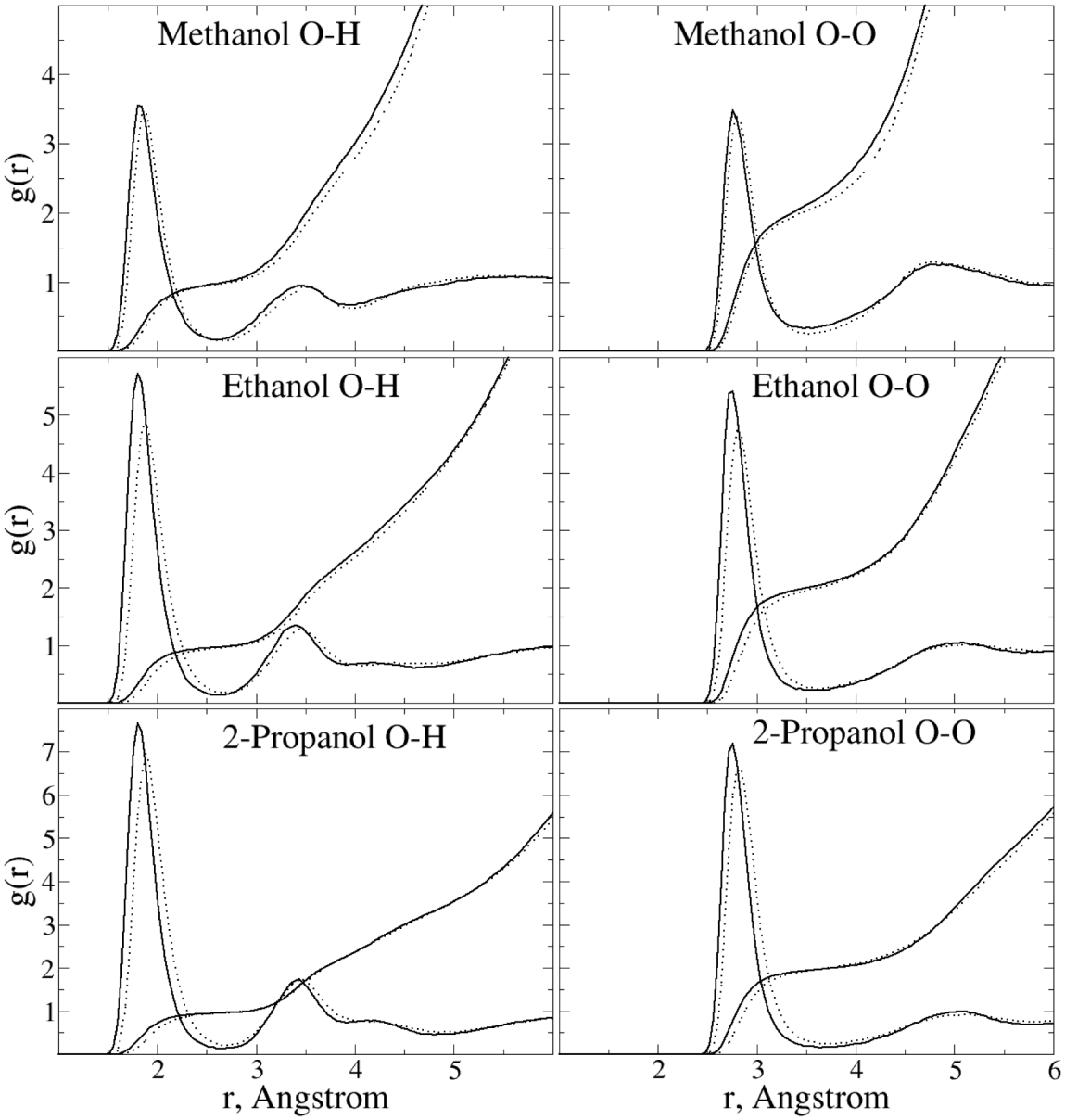

Figure 6.
Radial distributions functions of the pure solvents of ethanol and 2-propanol for both the CHARMM22 additive and Drude polarizable force fields. Results for the O-H (left panels) and O-O (right panels) intermolecular interactions are shown. Solid line: polarizable model; dotted line: CHARMM22 model.

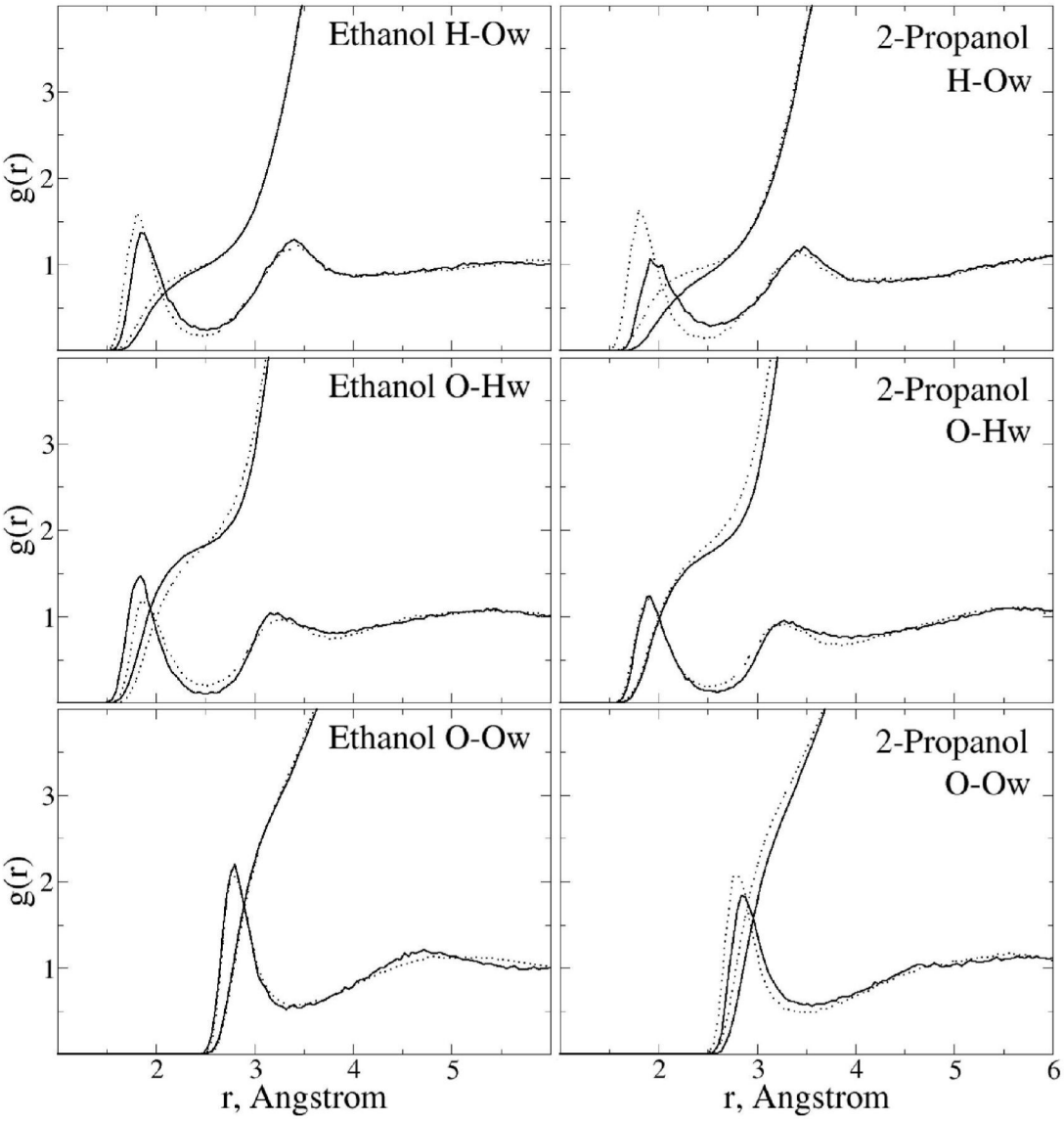

Figure 7.
Radial distributions functions of ethanol and 2-propanol in aqueous solution for both the CHARMM22 additive and Drude polarizable force fields. Solid line: polarizable model; dotted line: CHARMM22 model.

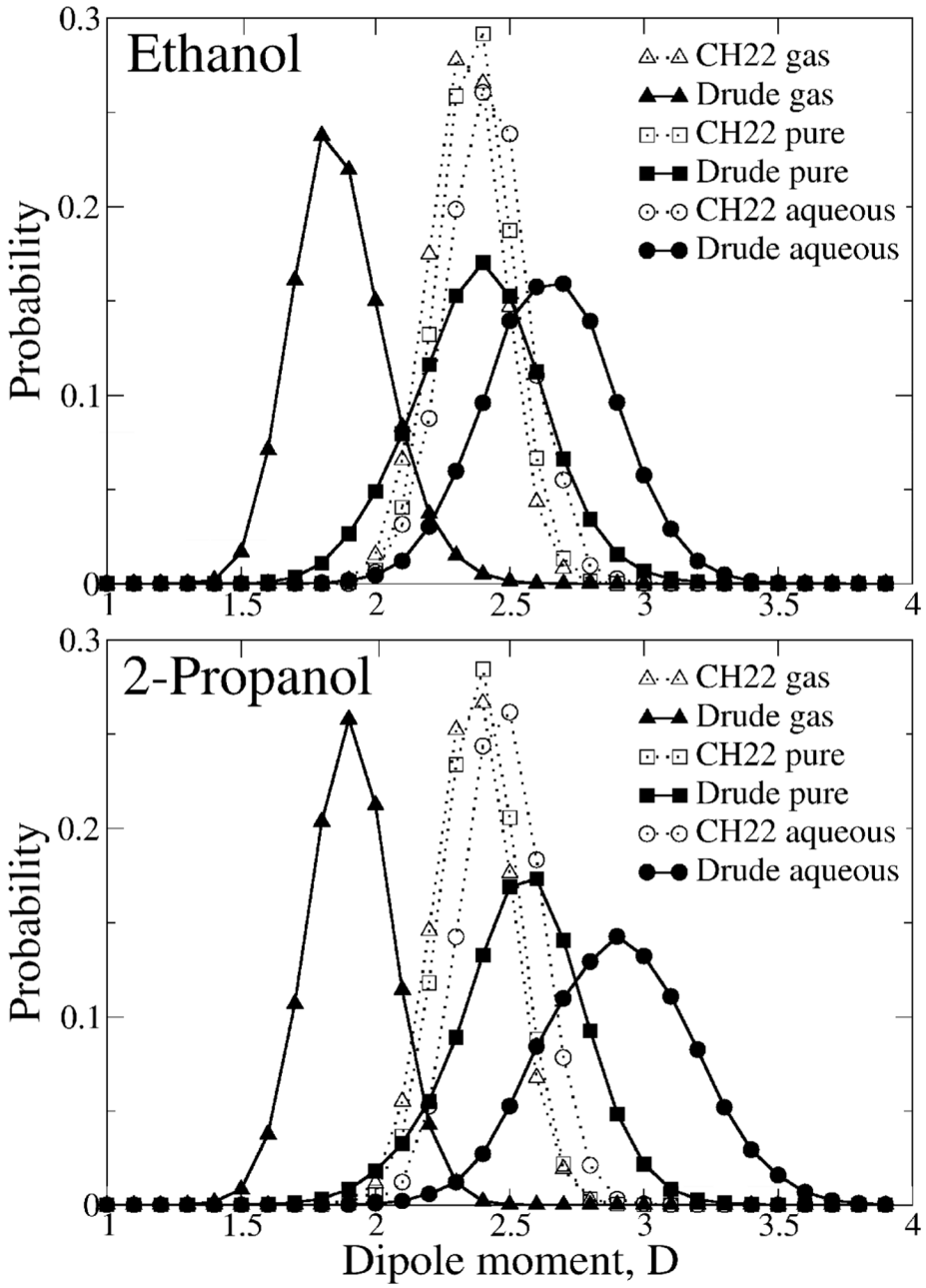

Figure 8.
Dipole moment distributions of ethanol and 2-propanol in the gas phase, in pure solvents and in aqueous solution for both the CHARMM22 additive and Drude polarizable force fields. Solid line: polarizable model; dotted line: CHARMM22 model.

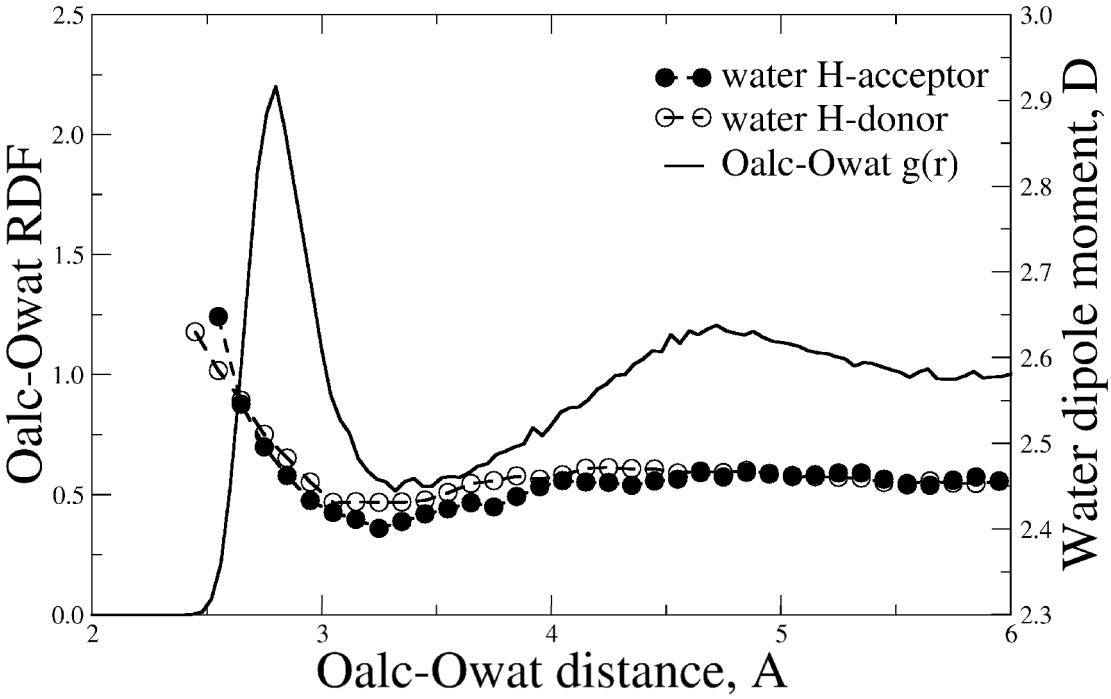

Figure 9.

Average water dipole moment around ethanol as a function of $O_{alcohol}$-O_{water} distance overlaid on the $O_{alcohol}$-O_{water} radial distribution function (solid line) of ethanol in water. Open circles indicate water molecules acting as H-bond donors and filled circles indicate water molecules acting as H-bond acceptors.

Table 1

Specification of Connolly surfaces for perturbation ion and grid point placement

Surface #	vdW scale factor	density factor	Dist. to atoms	Dist to pert. ions	Type
1[a]	1.3	5.0	0.0	0.0	Ions(bonds)
	1.3	5.0	1.4	2.0	Ions(gaps)
2	2.2	1.1	1.5	2.0	Ions(bonds)
	2.2	1.1	2.0	2.0	Ions(gaps)
3	4.0	0.1	2.0	2.0	Ions(bonds)
4[a]	1.3	6.0	0.0	2.0	Grids
5	2.2	1.1	1.0	2.0	Grids
6	3.0	1.3	1.0	2.0	Grids
7	5.0	0.6	1.0	2.0	Grids
8	6.0	0.2	1.0	2.0	Grids

[a]Only in vicinity of polar atoms

Table 2

Equilibrium geometries of alcohols in the trans conformations[a]

	Methanol		Ethanol		iso-Propanol		RMSD
	Drude	**Target**	**Drude**	**Target**	**Drude**	**Target**	
C-O[b]	1.43	1.40 (0.05)	1.43	1.42 (0.04)	1.43	1.43 (0.03)	0.02
C-C[c,e]	-	-	1.53	1.48 (0.05)	1.53	1.50 (0.03)	0.04
O-H[d]	0.97	0.97	0.97	0.97	0.97	0.97	0.00
C-H[d]	1.11	1.09	1.11	1.10	1.12	1.09	0.02
C-C-O[b]	-	-	111.4	111.5 (3.2)	110.4	109.7 (2.8)	0.5
C-C-C[b,e]	-	-	-	-	113.2	112.5 (2.6)	0.7
C-O-H[c]	107.6	107.4	107.5	107.6	106.7	106.6	0.1
H-C-O[c]	109.9	110.3	110.7	110.9	103.6	103.8	0.3
H-C-H,[cd]	109.1	108.6	107.3	107.6	-	-	0.4

[a] Bond lengths, Å; Valence angles, degrees; data are shown for carbon atom adjacent to oxygen.

[b] Cambridge crystallographic survey based on 2037 hits for methanol, 913 hits for ethanol, and 130 hits for iso-propanol; CSD version 5.27 (Nov 2005); standard deviations are shown in parentheses.

[c] MP2(fc)/6-31G(d) gas-phase optimized geometry.

[d] Not optimized; corresponding parameters were directly transferred from the polarizable alkanes.

Table 3

Alcohol-water minimum interaction energy differences relative to QM data.

	E_{QM} [a]	ΔE_{C22} [b]	$\Delta E_{Drude}2$	ΔE_{C22}, %	ΔE_{Drude}, %	$RRMS_{C22}$ [c]	$RRMS_{Drude}$ [c]
MeOH						0.44	0.19
BIS	−4.40	−1.83	−0.34	42	8		
180	−2.09	−2.29	−0.71	110	34		
120	−4.90	−1.12	−0.22	23	4		
ROH	−4.12	−2.09	−0.33	51	8		
EtOH						0.63	0.11
BIS	−4.82	−1.72	−0.70	36	15		
180	−2.33	−2.23	−0.50	96	21		
120	−4.80	−0.61	−0.52	13	11		
ROH	−4.24	−2.07	−0.39	49	9		
1-PrOH						0.69	0.12
BIS	−5.01	−1.38	−0.29	28	6		
180	−2.64	−1.86	−0.13	70	5		
120	−5.09	−0.21	−0.01	4	0		
ROH	−4.40	−1.95	−0.31	44	7		
2-PrOH						0.93	0.21
BIS	−4.68	−1.59	0.25	34	−5		
180	−2.46	−2.31	−0.24	94	10		
120	−4.76	0.16	0.13	−3	−3		
ROH	−3.99	−1.83	0.28	46	−7		

Energies in kcal/mol. See Figure 2 for interaction orientations. Results for the polarizable model include off-diagonal (i.e. NBFIX) $O_{alcohol}…O_{water}$ LJ parameters.

[a] QM calculations are performed at LMP2/cc-pvQZ//MP2/6-31G* level of theory.

[b] $\Delta E^{i}_{model} = E^{i}_{int}(model) - E^{i}_{int}(QM)$, where $E^{i}_{int}(model)$ is interaction energy corresponding to CHARMM22 or Drude models for i^{th} orientation.

[c] Relative RMS error calculated for the difference $\Delta E^{i}_{alcohol} - \Delta E^{ave}_{alcohol}$, where $\Delta E^{ave}_{alcohol}$ is the average difference between model and QM calculations for a given alcohol molecule.

Table 4

Alcohol-water minimum interaction distance differences relative to QM data.

	R_{QM} [a]	ΔR_{C22} [b]	ΔR_{Drude} [b]	ΔR_{C22},%	ΔR_{Drude},%	$RRMS_{C22}$ [c]	$RRMS_{Drude}$ [c]
MeOH						0.05	0.05
BIS	1.98	−0.14	−0.08	−7	−4		
180	2.12	−0.23	−0.14	−11	−7		
120	1.95	−0.11	−0.09	−6	−5		
ROH	1.95	−0.13	−0.01	−7	−1		
EtOH						0.06	0.04
BIS	1.98	−0.12	−0.09	−6	−5		
180	2.12	−0.24	−0.13	−11	−6		
120	1.97	−0.08	−0.10	−4	−5		
ROH	1.95	−0.13	−0.02	−7	−1		
1-PrOH						0.06	0.04
BIS	1.98	−0.12	−0.09	−6	−5		
180	2.12	−0.24	−0.13	−11	−6		
120	1.97	−0.08	−0.09	−4	−5		
ROH	1.95	−0.13	−0.02	−7	−1		
2-PrOH						0.07	0.04
BIS	1.97	−0.13	0.00	−7	0		
180	2.10	−0.23	−0.04	−11	−2		
120	1.96	−0.05	−0.01	−3	−1		
ROH	1.97	−0.09	0.06	−5	3		

Distance in Å, See Figure 2 for interaction orientations. Results for the polarizable model include off-diagonal (i.e. NBFIX) $O_{alcohol}$…O_{water} LJ parameters.

[a] QM calculations are performed at LMP2/cc-pvQZ//MP2/6-31G* level of theory.

[b] $\Delta R^{i}_{model} = R^{i}_{min}(model) - R^{i}_{min}(QM)$, where $R^{i}_{min}(model)$ is minimum energy distance corresponding to CHARMM22 or Drude models for i^{th} orientation.

[c] Relative RMS error calculated for the difference $\Delta R^{i}_{alcohol} - \Delta R^{ave}_{alcohol}$, where $\Delta R^{ave}_{alcohol}$ is the average difference between model and QM calculations for a given alcohol molecule.

Table 5

ESP Fitted atomic charges (q) and polarizabilities (α) of the model compounds

Atom	Methanol		Ethanol[a]		2-Propanol[a]	
	q	α	q	α	q	α
O	0.000	0.90	0.000	0.44	0.000	0.99
Lone-pair	−0.242	0.00	−0.231	0.00	−0.223	0.0
H (O)	0.352	0.00	0.355	0.00	0.365	0.0
C (O)	−0.006	1.92	−0.021	1.45	−0.003	1.08
H (CO)	0.046	0.00	0.064	0.00	0.084	0.00
C_{alk} (CH_2)	n/a	n/a	n/a	n/a	n/a	n/a
H_{alk} (CH_2)	n/a	n/a	n/a	n/a	n/a	n/a
C_{alk} (CH_3)	n/a	n/a	−0.18	2.05	−0.18	2.05
H_{alk} (CH_3)	n/a	n/a	0.06	0.00	0.06	0.00

n/a indicates not applicable

[a] Gauche- and trans-conformations were fitted simultaneously.

Table 6

Final atomic charges (q) and polarizabilities (α) of the model compounds

Atom	Methanol		Ethanol		2-Propanol		1-Propanol		2-Butanol	
	q	α	q	α	q	α	q	α	q	α
O	0.00	1.0	0.00	1.0	0.00	1.0	0.00	1.0	0.00	1.0
Lone-pair	−0.23	0.0	−0.23	0.0	−0.23	0.0	−0.23	0.0	−0.23	0.0
H (O)	0.36	0.0	0.36	0.0	0.36	0.0	0.36	0.0	0.36	0.0
C (O)	−0.14	1.0	−0.06	1.0	0.00	1.0	−0.06	1.0	0.00	1.0
H (CO)	0.08	0.0	0.08	0.0	0.10	0.0	0.08	0.0	0.10	0.0
C_{alk} (CH_2)	n/a	n/a	n/a	n/a	n/a	n/a	−0.12	1.2	−0.12	1.2
H_{alk} (CH_2)	n/a	n/a	n/a	n/a	n/a	n/a	0.06	0.0	0.06	0.0
C_{alk} (CH_3)	n/a	n/a	−0.18	1.4	−0.18	1.4	−0.18	1.4	−0.18	1.4
H_{alk} (CH_3)	n/a	n/a	0.06	0.0	0.06	0.0	0.06	0.0	0.06	0.0

n/a indicates not applicable.

Table 7

Dipole moments for alcohols in the trans-conformation

Alcohol	μ (C22)	μ (Drude)	μ (exp)	μ (QM)	Δμ (C22), %	Δμ (Drude), %
MeOH	2.38	1.83	1.70	1.72	40	8
EtOH	2.36	1.81	1.71	1.63	38	6
2-PrOH	2.43	1.87	1.58	1.73	54	18
2-BuOH	2.42	1.79	...	1.76	38	2
1-PrOH	2.35	1.82	1.55	1.54	52	17
1-BuOH	2.36	1.80	1.66	1.60	42	8
Average	n/a	n/a	n/a	n/a	44	10

Units in Debye. QM dipole moments at the MP2(fc)/aug-cc-pVQZ// MP2(fc)/6-31G(d) level. Percent differences with respect to the experimental data. Experimental data from [87].

Table 8

Pure solvent properties of neat alcohols

Property	MeOH[a]	EtOH	2-PrOH	2-BuOH	1-PrOH	1-BuOH
V_m(C22)	69.18 (0.34)	99.09 (0.31)	128.41 (0.39)	157.25 (0.56)	128.98 (0.40)	157.37 (0.42)
	2.90%	2.20%	0.50%	3.00%	3.40%	3.50%
V_m(Drude) final[b]	67.21 (0.15)	97.11 (0.19)	125.79 (0.30)	153.36 (0.32)	125.78 (0.20)	153.09 (0.49)
	0.00%	0.20%	−1.60%	0.50%	0.80%	0.70%
V_m(Drude) alternative[c]	66.02 (0.17)	95.42 (0.28)	124.11 (0.46)	152.13 (0.41)	124.06 (0.66)	151.87 (0.59)
	−1.8%	−1.5%	−2.9%	−0.3%	−0.6%	−0.1%
V_m(exp)	67.23	96.92	127.79	152.65	124.78	152.05
ΔH_{vap}(C22)	9.11 (0.04)	10.20 (0.05)	10.81 (0.06)	10.63 (0.33)	11.22 (0.29)	12.42 (0.27)
	1.80%	0.90%	−0.30%	−10.50%	−1.10%	−0.70%
ΔH_{vap}(Drude) final[b]	8.94 (0.04)	10.07 (0.06)	10.99 (0.07)	11.76 (0.18)	10.55 (0.13)	11.68 (0.19)
	−0.10%	−0.40%	1.20%	−1.00%	−7.00%	−6.60%
ΔH_{vap}(Drude) alternative[c]	9.58 (0.04)	10.86 (0.05)	11.83 (0.08)	12.51 (0.19)	11.36 (0.13)	12.49 (0.19)
	+7.0%	+7.4%	+9.0%	+5.3%	+0.2%	−0.1%
ΔH_{vap}(exp)	8.95	10.11	10.85	11.88	11.34	12.51

Heats of vaporization in kcal/mol and molecular volumes in $Å^3$; values in parenthesis are the standard deviations; percent differences are with respect to experiment. Experimental data from [87].

[a] Methanol LJ well-depth: Carbon ε=0.11, Hydrogen ε=0.035.

[b] Final polarizable model Oxygen LJ ε=0.15, R=1.765.

[c] Alternative polarizable model Oxygen LJ ε=0.15, R=1.74.

Table 9

Differences between empirical and QM values and RMS fluctuations about the average differences and ratios for the rare gas interactions with methanol and ethanol.

Orientation **CHARMM22**	**MeOH+He** ΔR_{min}	ΔE_{int}	**MeOH+Ne** ΔR_{min}	ΔE_{int}	**EtOH+He** ΔR_{min}	ΔE_{int}	**EtOH+Ne** ΔR_{min}	ΔE_{int}
BIS	−0.12	−0.01	0.03	0.15	−0.18	−0.03	0.02	0.26
180	0.03	0.02	0.14	0.23	0.00	0.02	0.12	0.25
120	−0.32	−0.03	−0.08	0.16	−0.36	−0.06	−0.10	0.17
ROH	−0.33	0.01	−0.16	0.37	−0.36	0.01	−0.15	0.38
CH3	0.19	0.06	0.20	0.34	0.00	0.02	0.10	0.37
CH2	n/a	n/a	n/a	n/a	−0.15	−0.01	0.03	0.28
RMS	0.20	0.03	0.15	0.10	0.15	0.03	0.10	0.07
Drude	ΔR_{min}	ΔE_{int}	ΔR_{min}	ΔE_{int}	ΔR_{min}	ΔE_{int}	ΔR_{min}	ΔE_{int}
BIS	−0.14	−0.02	−0.03	0.11	−0.20	−0.02	−0.04	0.23
180	0.02	0.02	0.10	0.22	0.00	0.02	0.10	0.24
120	−0.33	−0.04	−0.13	0.12	−0.39	−0.05	−0.16	0.15
ROH	−0.35	0.01	−0.28	0.28	−0.37	0.01	−0.28	0.31
CH3	0.16	0.03	0.17	0.29	−0.02	0.01	0.08	0.37
CH2	n/a	n/a	n/a	n/a	−0.26	−0.03	−0.08	0.23
RMS	0.20	0.03	0.16	0.08	0.15	0.03	0.13	0.07

Interaction energy differences (kcal/mol) and distance differences (Å) are calculated as X^{model}-X^{QM}.

Table 10

Dielectric constant

Alcohol	C22[2]	Drude, ε_∞ [a]	Drude, ε [b]	Exp., ε [b]
MeOH	17.2 (0.1)	1.5	30.1 (0.1)	32.61
EtOH	18.8 (0.3)	1.6	21.4 (0.2)	24.85
2-PrOH	13.7 (0.1)	1.7	17.6 (0.5)	19.26
2-BuOH	7.8 (0.1)	1.7	15.8 (0.4)	15.94
1-PrOH	15.2 (0.2)	1.6	19.5 (1.1)	20.52
1-BuOH	10.8 (0.1)	1.7	21.2 (0.7)	17.33
Ave. % diff.	−35.9	n/a	−2.3	n/a

[a] ε_∞ estimation from the Clausius-Mossotti equation using experimental polarizabilities of alcohols.

[b] T=298.15K; Experimental data from [87]. Ave. % diff. is the average of the percent difference with respect to experiment over the six alcohols studied.

Table 11

Self-diffusion coefficients of alcohols, (D_{tot}), 10^{-5} cm^2/s

Alcohol[a]	D_{PBC} C22	Drude	D_{corr}	D_{tot} C22	Drude	Exp.
MeOH	2.16 (0.16)	2.03 (0.44)	0.56	2.72	2.59	2.4
EtOH	1.08 (0.15)	0.93 (0.13)	0.25	1.33	1.18	1.0
2-PrOH	0.60 (0.13)	0.52 (0.07)	0.12	0.72	0.64	0.6
1-PrOH	0.66 (0.13)	0.66 (0.16)	0.13	0.79	0.79	0.6

[a] Data calculated as in reference: methanol[21, 88–90], ethanol, [22, 88–91] iso-propanol,[89,90] n-propanol. [89–91] D_{pbc} is the direct result obtained from MD simulation involving periodic boundary condition; D_{corr} is the correction for system-size effect according to eq. 4.

Table 12

Isothermal compressibility of alcohols, MPa^{-4}

Alcohol	Temp., K	C22	Drude	Exp.[a]
MeOH	313.15	11.98 (0.96)	8.68 (0.97)	13.83
EtOH	293.15	10.12 (1.08)	10.03 (0.69)	11.19
EtOH	343.15	15.24 (1.44)	16.58 (1.53)	15.93
2-PrOH	313.15	13.62 (2.13)	11.71 (1.42)	13.32
1-PrOH	273.15	8.73 (0.99)	8.17 (1.01)	8.43

[a] Experimental data from reference 87.

Table 13

Free energies of solvation, kcal/mol

Alcohol	CHARMM22 LRC[a]	ΔG_{solv}	%diff	Drude LRC[a]	ΔG_{uncorr}	ΔG_{solv}	%diff	Exp ΔG_{solv}
MeOH	−0.20	−4.98 (0.08)	−3	−0.26	−5.20 (0.19)	−4.64 (0.18)	−9	−5.11[b]
EtOH	−0.31	−5.34 (0.12)	7	−0.35	−5.66 (0.31)	−4.97 (0.13)	−1	−5.01[b]
2-PrOH	−0.39	−5.07 (0.09)	7	−0.45	−6.06 (0.23)	−4.82 (0.16)	1	−4.76[b]
2-BuOH	−0.45	−4.93 (0.27)	8	−0.57	−6.11 (0.18)	−4.75 (0.43)	4	−4.57[c]
1-PrOH	−0.42	−5.33 (0.24)	10	−0.46	−5.38 (0.16)	−4.85 (0.15)	0	−4.83[b]
1-BuOH	−0.53	−5.60 (0.21)	19	−0.57	−5.72 (0.16)	−4.67 (0.23)	−1	−4.72[b]
Aver			9				−1	

[a] The long range correction (LRC) is estimated for dispersion forces. In the polarizable model, ΔG_{uncorr} represents free energy obtained using standard combining rule for intermolecular LJ interactions and ΔG_{solv} is free energy that included an off-diagonal (i.e. NBFIX) for the $O_{alcohol}\cdots O_{water}$ LJ parameters (R_{min}=3.60, ε=0.18 for primary alcohols, and R_{min}=3.60, ε=0.21 for secondary alcohols).

[b] Experimental results as reported in reference 92

[c] reference.93